Journal of Materials Chemistry A

REVIEW

View Article Online
View Journal | View Issue

Cite this: *J. Mater. Chem. A*, 2019, **7**, 25691

Janus electrochemical exfoliation of two-dimensional materials

Yiyun Fang,†[ab] Xinzhe Li, †[ab] Jing Li,[b] Chuanhao Yao, *[c] Hui Ying Hoh,[a] Xiao Hai,[b] Jiong Lu*[b] and Chenliang Su *[a]

Atomically thin two-dimensional (2D) materials have attracted increasing research interest due to their fascinating properties as well as multifarious potential applications. Despite tremendous achievements, the fundamental challenge in this rapidly growing field is fabricating these 2D materials with a well-controlled structure in an effective and scalable way. Electrochemical exfoliation, where bulk crystals can be electrochemically positively/negatively charged using intercalators, is an ingenious strategy to prepare high-quality 2D materials with Janus characteristics for a wide range of applications: on the one hand, the exfoliated 2D materials by cathodic exfoliation *via* cation intercalation under a reductive environment can possess advantages such as large size, high crystallinity, and a pure phase structure; on the other hand, by using anodic exfoliation *via* anion intercalation, surface modifications or oxidations could occur, which allows production of atomically thin 2D materials with diverse functionalities. This review article focuses mainly on the state-of-the-art developments in the smart and effective production of different categories of atomically thin 2D materials by cathodic and anodic electrochemical exfoliation, herein named as "Janus electrochemical exfoliation". The design strategies to realize Janus exfoliation of bulk crystals, the interfering factors such as intercalators, and the exfoliation mechanism are comprehensively summarized and discussed. More importantly, applications of these electrochemically exfoliated 2D materials in optoelectronic devices, energy storage, biosensing and catalysis are also detailed. Finally, the perspectives on the challenges and opportunities of this promising field are presented.

Received 23rd September 2019
Accepted 24th October 2019

DOI: 10.1039/c9ta10487a

rsc.li/materials-a

[a]*SZU-NUS Collaborative Center and International Collaborative Laboratory of 2D Materials for Optoelectronic Science & Technology of Ministry of Education, Engineering Technology Research Center for 2D Materials Information Functional Devices and Systems of Guangdong Province, Institute of Microscale Optoelectronics, Shenzhen University, Shenzhen 518060, China. E-mail: chmsuc@szu.edu.cn*

[b]*Department of Chemistry, National University of Singapore, 3 Science Drive 3, Singapore 117543, Singapore. E-mail: chmluj@nus.edu.sg*

[c]*Shaanxi Key Laboratory of Flexible Electronics (KLoFE), Institute of Flexible Electronics, Northwestern Polytechnical University, Xi'an 710072, China. E-mail: iamchyao@nwpu.edu.cn*

† These authors contributed equally to this review.

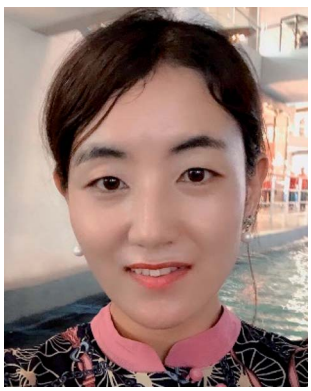

Yiyun Fang received her PhD degree in Physical Chemistry in 2017 from the Lanzhou University of China. Then, she started her postdoc careers at the SZU-NUS Collaborative Center and International Collaborative Laboratory of 2D Materials for Optoelectronic Science & Technology of Ministry of Education in Shenzhen University. From 2018, she has been working as a visiting research fellow in the research group of Prof. Lu Jiong at the Department of Chemistry, National University of Singapore. Her current research interest focuses on electrochemically exfoliated 2D materials for catalytic application.

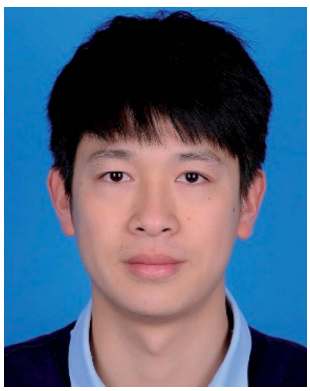

Xinzhe Li obtained his PhD degree at Lanzhou University/China in 2017. After that, he continued his research career as a visiting research fellow at the Department of Chemistry, National University of Singapore, under a collaborative research program with the SZU-NUS Collaborative Center and International Collaborative Laboratory of 2D Materials for Optoelectronic Science & Technology. Now, he is a postdoctoral research fellow at the National University of Singapore. His current research interest focuses on the electrochemical exfoliation of 2D materials and atomically precise synthesis of single atom/cluster catalysts for energy related conversion.

1. Introduction

The discovery of graphene *via* mechanical exfoliation by Novoselov, Geim, and co-workers[1] has ignited research enthusiasm in two-dimensional (2D) materials. This heightened interest is due to the innovative physical, chemical, optical, and electronic features possessed by 2D materials, as well as their potential in a wide range of applications.[2–10] To date, various 2D nanomaterials beyond graphene have been investigated, such as black phosphorus (BP),[11,12] transition metal dichalcogenides (TMD),[13–15] layered double hydroxides,[16,17] metal phosphorus trichalcogenides (MPTs),[18–20] metal–organic frameworks (MOFs),[21–23] covalent organic frameworks (COFs)[24–26] and perovskites.[27,28] The presence of exposed surfaces in 2D materials means that their thickness and the amount of surface defects or absorbents can dramatically influence their chemical or physical properties, and controllable fabrication of 2D materials with a desired thickness or surface structure is a prerequisite for meaningful research or application.

Generally, two strategies are employed to fabricate monolayer or few-layer 2D materials: (1) bottom-up methods, such as chemical vapor deposition (CVD) or hydrothermal synthesis,[29–32] can realize accurate control from the growth source, allowing the synthesis of 2D materials with a desired morphology, thickness and hetero-/doping-structures. However, the high cost of maintaining high temperature and vacuum conditions limit the application of CVD-produced materials to thin film devices. In contrast, 2D materials obtained *via* hydrothermal synthesis usually suffer from inferior quality and limited size, and thus are not suitable for use in photonic or electronic devices. Moreover, the scale-up of the hydrothermal method is another thorny challenge. (2) The top-down methods, such as mechanical exfoliation by Scotch tape,[33–35] liquid exfoliation,[36–39] and electrochemical exfoliation,[40–43] utilize bulk crystals to fabricate atomically thin 2D materials. Due to the different bonding strengths of in-plane covalent bonding and interlayer van der Waals (vdW) bonding, the vdW bonding can be preferentially broken *via* an external force or intercalation, leading to the isolation of 2D flakes. Among the top-down methods, mechanical exfoliation can prepare atomically thin 2D materials with high crystallinity. However, the relatively low yield of thin flakes makes this method applicable exclusively in laboratories for fundamental research. In liquid exfoliation, solvents or surfactants can be intercalated into the interlayer space of layered materials through sonication or vortex forces, resulting in the expansion or exfoliation of layered materials. This method is facile, scalable and universal for almost all kinds of layered materials. However, the as-exfoliated flakes are of relatively small sizes (average ~100 nm). Electrochemical intercalation, a category of liquid exfoliation, employs an applied voltage or current to drive

Chuanhao Yao received his PhD degree from the Institute of Solid State Physics, Chinese Academy of Sciences, in 2016. After that he worked as a postdoctoral research fellow at the Department of Chemistry, National University of Singapore. He currently is a professor at the Institute of Flexible Electronics, Northwestern Polytechnical University. His interests focus on ultrafine nanomaterials such as atomically precise metal nanoclusters and two dimensional nanomaterials for electrocatalysis including oxygen reduction, oxygen evolution, hydrogen evolution, and CO_2 as well as N_2 electrochemical fixation.

Dr. Jiong Lu is currently an assistant professor at the Department of Chemistry, Centre for Advanced 2D Materials, National University of Singapore (NUS). He received his Bachelor's degree from Fudan University (China) in 2007 and PhD degree from the NUS in 2011. After that, he worked as a postdoc fellow in the Graphene Research Centre, NUS, and then joined Mike Crommie's group at the Department of Physics, UC, Berkeley, for his postdoctoral research. His current research interests include atomic-scale imaging and characterization of 2D materials and their gate-tunable devices, and single-atom catalysis for energy related applications. He has published more than 50 peer-reviewed papers with a total citation of over 3900 citations.

Chenliang Su received his BS degree (2005) and PhD degree (2010) from the Department of Chemistry at the Zhejiang University of China. After that he worked as a research fellow at the Advanced 2D Materials and Graphene Research Centre at the National University of Singapore (2010–2015). He is now a full-professor at the International Collaborative Laboratory of 2D Materials for Optoelectronics Science and Technology (ICL-2D MOST), Shenzhen University, and a Principal Investigator of the ICL-2D MOST in materials science. His current interests focus on the chemical design of two dimensional materials/nano-materials for catalysis and energy related applications.

the counterions into the interlayer space of layered materials, and thus the efficiency of intercalation and delamination of layered materials is greatly enhanced. This method dates back to 1841 when graphite intercalation compounds (GICs) were first reported by Schafhaeutl *et al.*[44] Later, in 1926, alkali metals, such as K, were successfully incorporated into graphite as GICs by Cadenbach *et al.*[45] Inspired by this discovery, Rüdorff and Hofman used electro-intercalation approaches to prepare sulfuric acid GICs in 1938.[46] In this process, a fixed potential or electrical current was applied to the solution. As a result, the ionic species were intercalated into the layers of a graphite crystal, weakening the interlayer force and significantly expanding the tightly stratified bulk crystal, thereby facilitating the separation of graphene sheets and consequently the release of 2D sheets into the solution. Following this work, research activity in electrochemically produced GICs grew.

Electrochemical exfoliation has been applied to successfully exfoliate many bulk crystals into atomically thin 2D materials (Fig. 1a). This method is facile, scalable, low-cost and has a high yield. The overall process first involves application of a fixed voltage or electrical current to a bulk crystal, leading to the intercalation of ionic species into the interlayer space. Subsequently, anodic/cathodic degradation of intercalants into gaseous species leads to dramatic volumetric expansion forces in the galleries, resulting in the ready exfoliation of 2D flakes. It should be noted that the types of applied voltage and electrolyte play a crucial role in this process. They affect not only the efficiency of the exfoliation but also the quality and properties of the exfoliated materials. Depending on the type of voltage applied, electrochemical exfoliation can be further classified into anodic and cathodic strategies.[43,47] The former involves applying a positive bias to the bulk crystal to attract negatively charged ions (anions) in the solution, along with any co-intercalating molecules, while the latter uses a negative bias to intercalate positively charged ions (cations) and any co-intercalating species in the reaction mixture into bulk crystals. Generally, anodic intercalation is accompanied by an abundance of oxidative radicals and a rigorous reaction, leading to not only a quick intercalation process but also the formation of structure defects or covalent functional groups in the 2D flakes. Cathodic intercalation is much gentler, thus allowing thorough intercalation, although at a slower rate. The 2D

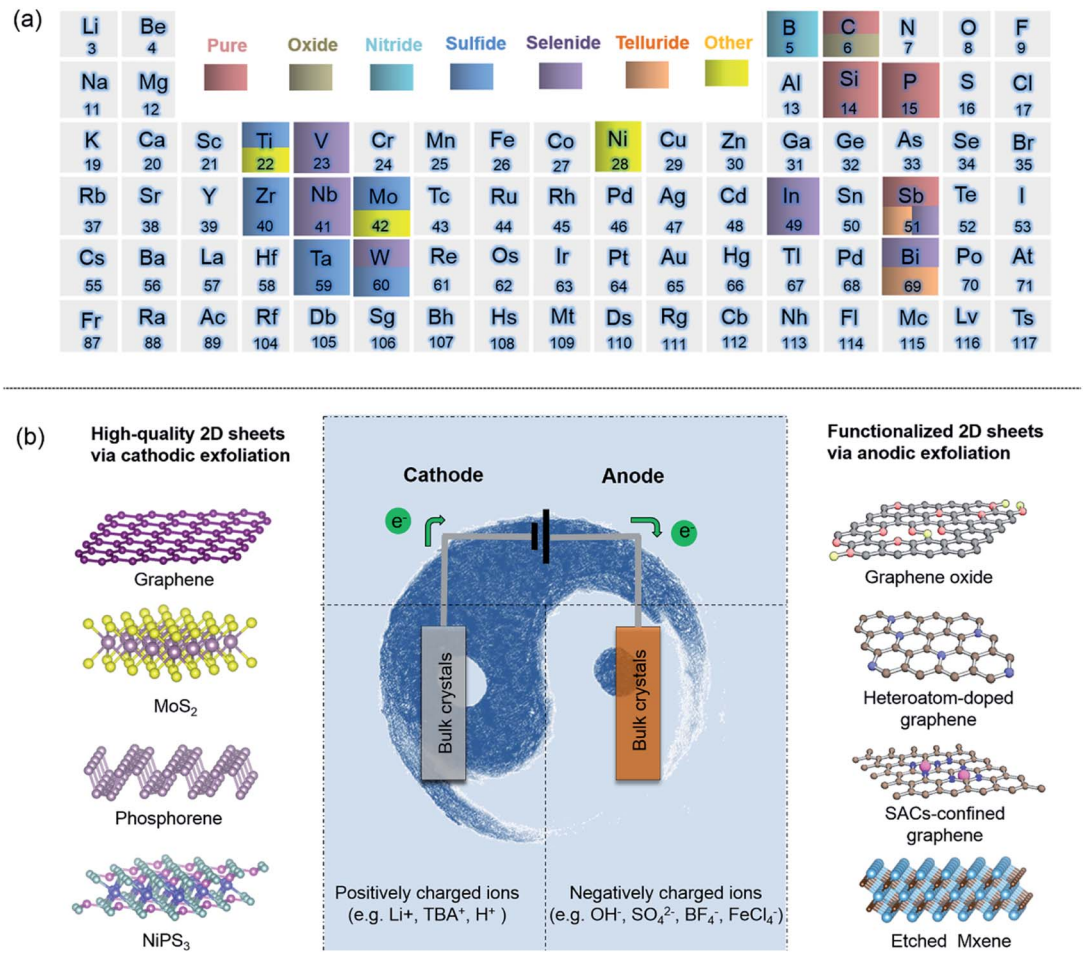

Fig. 1 (a) Reported 2D materials obtained by electrochemical exfoliation to date. (b) Schematic overview of cathodic and anodic exfoliation to prepare ultrathin 2D materials with Janus features. A positive or negative charge is created at the working electrode, attracting oppositely charged intercalating ions (middle). Typical high-quality 2D sheets obtained *via* cathodic exfoliation (left) and functionalized 2D sheets *via* anodic exfoliation (right) are also presented.

materials obtained by cathodic exfoliation usually possess large size, high crystallinity, and a pure phase structure, comparable with the products from the CVD method. Therefore, by precisely controlling the electrochemical exfoliation process, high quality ultrathin 2D materials with an intact atomic structure or sheets with tailored functionalities can be prepared (Fig. 1b). In this review, we systematically summarize the reported 2D materials obtained by electrochemical exfoliation to date and discuss the effects on the Janus electrochemical exfoliation of different bulk crystals to fabricate targeted 2D materials. Special attention will be paid to the type of intercalator and the exfoliation mechanism. The superiority of exfoliated 2D sheets and practical applications will be summarized and discussed.

2. Cathodic exfoliation

As mentioned above, cathodic exfoliation signifies the application of a negative voltage to bulk crystals, which drives the intercalation of cations in electrolyte. Generally, solvated cations are the actual intercalants into bulk crystals and ignite the expansion process. The cathodic exfoliation *via* intercalation of positive ions originates from the Li-intercalating strategy used in batteries (xLi + TiS_2 → Li_xTiS_2).[48] When a negative electric field is applied, the bulk crystals will be intercalated with Li^+ and completely transformed into the intercalated compound. During this process, the interlayer distance can be efficiently expanded, and the vdW interactions between the layers are weakened. After the ultrasonication of the intercalated compound in a solvent, such as water and ethanol, the metallic Li formed by the reduction of electrons can react with water (Li + $2H_2O$ → $2LiOH + H_2$), forming H_2 gas, which can further separate the individual layers.[49] Inspired by the case of inserting Li^+ between the layers of a material, Wang *et al.* successfully employed $LiClO_4$ in propylene carbonate to exfoliate graphite into graphene sheets.[50] As a result, highly conformal coatings of conductive films (15 ohms per square at a graphene loading of <1 mg cm^{-2}) on commercial paper could be fabricated by using dispersible graphene ink. Afterward, Zhang's group demonstrated an ingenious strategy to prepare other single-layer 2D nanosheets, such as 2D MoS_2, WS_2, TiS_2, TaS_2, and ZrS_2, by precisely controlling the lithium intercalation and subsequent exfoliation using the cut-off voltage (Fig. 2a).[51] During this process, the lithium inserted in the interlayer space of layers was precisely manipulated to prevent the decomposition of the lithium-intercalated compounds. Following this work, few-layer h-BN, $NbSe_2$, WSe_2, Sb_2Se_3, and Bi_2Te_3 were also prepared.[52] The dispersions and atomic force microscopy (AFM) images of single-layer MoS_2, WS_2, TiS_2, TaS_2 and ZrS_2, and few-layer $NbSe_2$ nanosheets are summarized in Fig. 2b, indicating the universality of cathodic exfoliation *via* Li-intercalation for the preparation of 2D nanosheets. Recently, few-layer silicene nanosheets were also synthesized by using electrochemical Li-intercalation.[53]

Though bulk layered crystals can be exfoliated *via* Li-intercalation, the presence of a large amount of Li^+ ions may induce an undesired phase transition into the host crystal and make the subsequent product unsuitable for application in electronic devices. For example, 2H-MoS_2 nanosheets obtained by Li^+ ion intercalation are usually mixed with the metallic 1T phase. As a result, the mobility is only about 0.3 cm^{-2} V^{-1} S^{-1}, and the on/off ratio is less than 10. Besides, these MoS_2 nanosheets have a very broad thickness distribution, leading to the poor electrical performance of the thin-film materials: mobility is about 0.4 cm^{-2} V^{-1} S^{-1}, and the on/off ratio is about 100. Thus, synthesis of solution-processable 2D nanosheets with high-quality remains a huge challenge.

An alternative to prevent electrons from injecting into the 2D crystals, which may cause the undesired phase transition, is to supersede the small size Li^+ ions (diameter $d \approx 2$ Å) with larger cations. Unlike alkali ions, quaternary ammonium cations, such as tetra-methyl-ammonium (TMA^+, 0.56 nm), tetra-ethyl-ammonium (TEA^+, 0.67 nm), and tetra-*n*-butyl-ammonium (TBA^+, 0.83 nm), generally exhibit large diameters. For example, Copper *et al.* demonstrated that TBA^+ was an effective cation for the expansion of highly oriented pyrolytic graphite (HOPG).[54] By extending this discovery, Lin *et al.* proved that electrochemical cathodic exfoliation of bulk MoS_2 crystals with the aid of tetraheptylammonium bromide (THAB) could generate solution-processable, phase-pure semiconducting 2H-MoS_2 nanosheets with high uniformity.[42] During the exfoliation process, THA^+ cations, driven by a negative electrochemical potential, were inserted into the MoS_2 layers, causing a substantial augmentation in the interlayer spacing of the MoS_2 crystals. AFM results of the exfoliated MoS_2 nanosheets revealed that the thickness distribution was 3.8 ± 0.9 nm and the lateral dimension was 0.5–2 μm (Fig. 3b–d). Moreover, X-ray photoelectron spectroscopy (XPS) results indicated that the 1T phase was dominant in the Li-exfoliated MoS_2 nanosheets; however, the THAB-exfoliated MoS_2 nanosheets contained the pure 2H phase (Fig. 3g). When used as thin-film transistors, these exfoliated MoS_2 nanosheets demonstrated high room-temperature mobilities (~10 cm^{-2} V^{-1} S^{-1}) and on/off ratios (10^6) (Fig. 3h and i), substantially exceeding those of previously reported MoS_2 thin-film transistors (Table 1). Due to the successful large-scale preparation of solution-processable 2H phase MoS_2 *via* electrochemical exfoliation, functional logic gates and computational circuits can be constructed. Moreover, this THAB-inserting strategy *via* electrochemistry could be employed to fabricate other high-quality 2D materials, such as WSe_2, Bi_2Se_3, $NbSe_2$, In_2Se_3, Sb_2Te_3, and BP, revealing its promising application for fabricating multifarious 2D materials.

Though significant development was achieved, the mechanism of electrochemical exfoliation of MoS_2 crystals is not mentioned. Zhang *et al.* fabricated large semiconducting MoS_2 sheets (~50 μm) with an intact crystalline structure by the cathodic exfoliation approach in tetra-*n*-butylammonium bisulfate/propylene carbonate electrolyte.[55] In their proposed exfoliation mechanism, the variable diameters of TBA^+ cations (0.47 nm for the flattened configuration and 0.89 nm for the tetrahedral configuration) could realize the expansion of the interlayer spacing of MoS_2 foil to a maximum gallery of 0.89 nm. During this process, the migration and subsequent reduction of H^+ to produce hydrogen bubbles are essential to overcome the

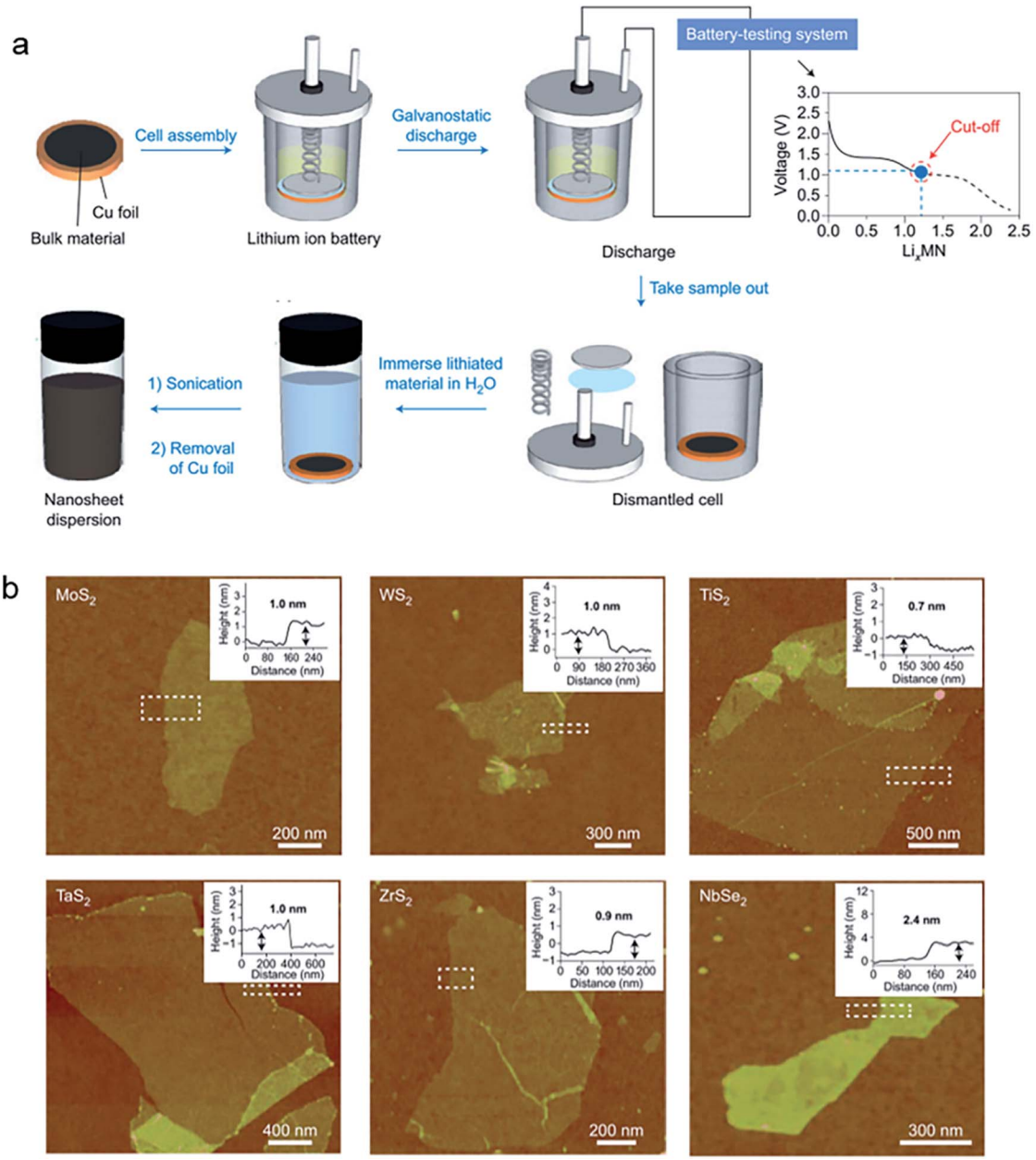

Fig. 2 Fabricated ultrathin 2D nanosheets *via* employing alkali metal ions as intercalators for electrochemical exfoliation. (a) Schematic illustration of the fabrication of 2D nanosheets. (b) AFM images of 2D MoS_2, WS_2, TiS_2, TaS_2, ZrS_2, and $NbSe_2$ on SiO_2 substrates. Reproduced from ref. 14 with permission from Nature Publications, copyright 2013.

van der Waals interactions and further enlarge the gaps between adjacent layers (eqn (1)–(3)).

$$TBA{\cdot}HSO_4 \leftrightarrow TBA^+ + HSO_4^- \quad (1)$$

$$HSO_4^- \leftrightarrow SO_4^{2-} + H^+ \quad (2)$$

$$2H^+ + 2e^- \rightarrow H_2 \quad (3)$$

The cathodic reduction also can possibly transform TBA^+ into other species (eqn (4)–(6)).[56] Thus, the large volume expansion combined with gas release overcomes the weak interactions between the layers.

$$(n\text{Butyl})_4N^+ + e^- \rightarrow (n\text{Butyl})_4N^{\bullet} \quad (4)$$

$$(n\text{Butyl})_4N^{\bullet} \rightarrow n\text{Butyl}^{\bullet} + (n\text{Butyl})_3N^{\bullet} \quad (5)$$

$$n\text{Butyl}^{\bullet} + e^- \rightarrow n\text{Butyl}^- \quad (6)$$

Later, by restacking the exfoliated MoS_2 flakes on a polyimide substrate, a flexible sensor device with a large area (60 × 60 μm) was assembled, which demonstrated a low detection limit (in the femtomolar–picomolar range).

The high quality of cathodic exfoliation can be further verified by the successful exfoliation of several air-sensitive

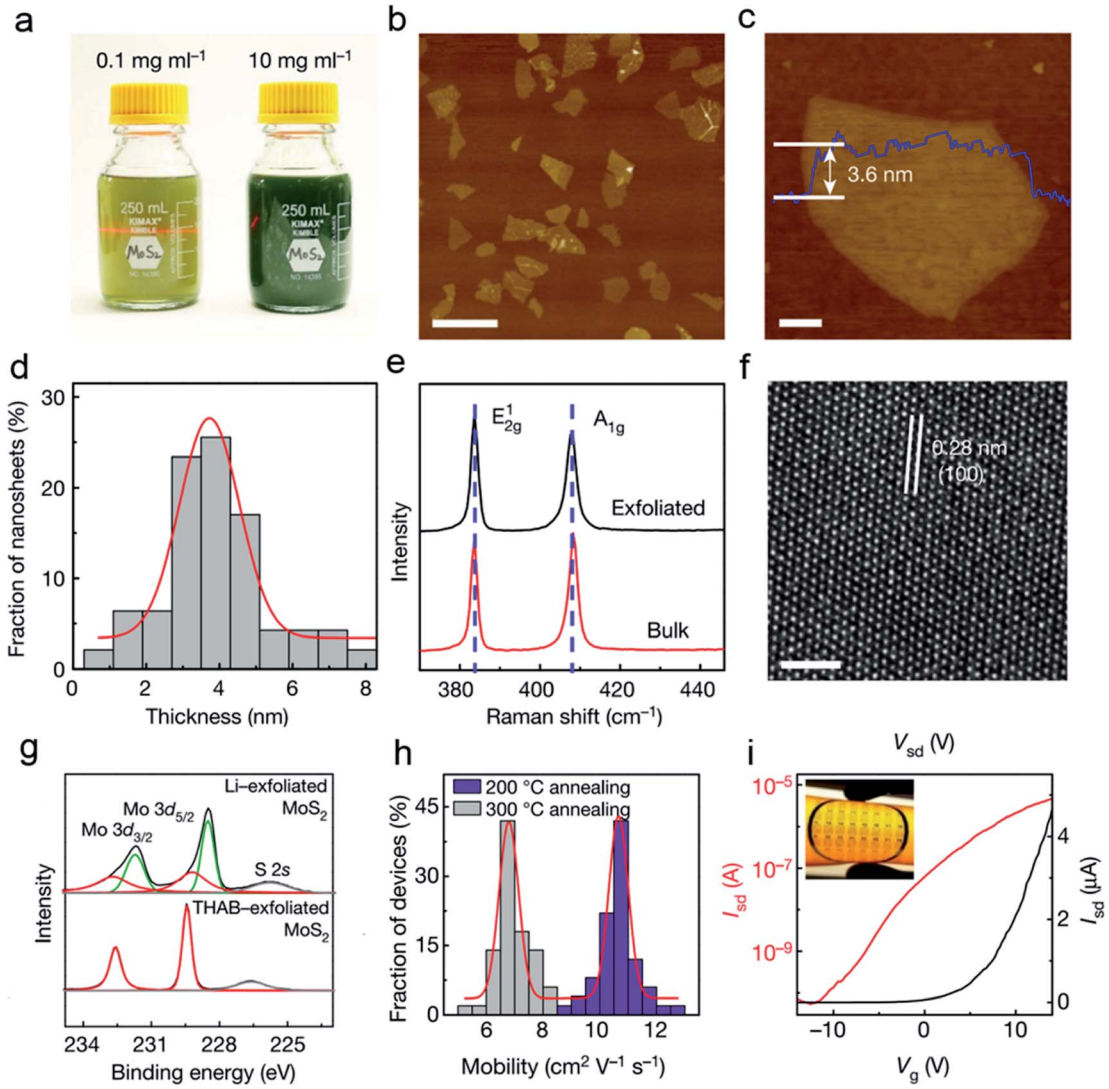

Fig. 3 Electrochemical cathodic exfoliation to prepare atomically thin 2D MoS_2 nanosheets with high quality. (a) Photograph of exfoliated MoS_2 nanosheets at different concentrations. (b) AFM image of multitudinous MoS_2 nanosheets. Scale bar, 2 μm. (c) The thickness of an individual exfoliated MoS_2 sheet. (d) Statistical data of AFM (bars) results and a Gaussian fit (red line) of exfoliated MoS_2 nanosheets. (e) Raman spectroscopy results of the exfoliated MoS_2 nanosheets (top, black), and of the bulk crystals for reference (bottom, red). (f) The high-resolution TEM (HRTEM) image of a single MoS_2 nanosheet. (g) XPS spectra of THAB-exfoliated MoS_2 and Li-exfoliated MoS_2. (h) The statistical distribution of mobility for 50 individual transistors annealed at 200 °C (purple bars) and at 300 °C (grey bars). The red curves are Gaussian fits. (i) MoS_2 thin-film transistors assembled on a flexible substrate. Reproduced from ref. 42 with permission from Nature Publications, copyright 2018.

materials. Phosphorene is another promising 2D material that has attracted intense interest in recent years.[75] Different from graphene and MoS_2, which display no bandgap and direct bandgaps only in the monolayer form,[13,76] respectively, this fancy material exhibits a direct bandgap of ~1.5 eV for monolayer phosphorene and ~0.3 eV for bulk BP.[77,78] Thus, BP has been extensively investigated for application in both electronics and optoelectronics, such as transistors,[11,79,80] photodetectors,[81] and solar cells.[82] Nevertheless, due to the fast degradation of thin flake BP in air, the ordinary exfoliation process including both mechanical and solution exfoliation methods are all carried out in a glovebox or under an inert gas atmosphere, which severely limits the research of phosphorene on the 2D scale.

Huang *et al.* used tetrabutylammonium hexafluorophosphate as a cationic intercalator for electrochemical cathodic exfoliation to fabricate phosphorene without surface functional groups.[83] What's more, the number of layers of phosphorene can be controlled from 2 to 11 layers by adjusting the applied potential. When used directly as an anode material in a sodium-ion battery, it presented a capacity of 1968 mA h g^{-1} at a current density of 100 mA g^{-1}. Yang *et al.* also demonstrated an electrochemical delamination strategy, which effectively exfoliated bulk BP crystals into large (~20.6 mm), defect-free, few-layer flakes with a high exfoliation yield (~78%).[84] The authors summarized three key factors that were responsible for the effective intercalation and exfoliation: (1) the variable vertical diameter of flexible *n*-butyl chains (0.47–0.89 nm)

Table 1 Comparison of device performance at room temperature for MoS_2 semiconductor thin films[a]

Synthesis method	Intercalator	Thickness (nm)	Processing temperature (°C)	Mobility ($cm^2 V^{-1} s^{-1}$)	On/off ratio	Ref.
Electrochemical exfoliation	**Quaternary ammonium bromide**	**3.6**	**300**	**7–11**	**10^6**	42
Electrochemical exfoliation	$LiPF_6$	~1	50	<0.3	<2	57
Ultrasonic exfoliation	1,2-Dichlorobenzene	N/A	25	0.02	N/A	58
Ultrasonic exfoliation	NMP	~14 layers	70	0.15	10^2	59
Ultrasonic exfoliation	DMF	5–7	450	<0.1	<10	60
Wet chemistry	N/A	N/A	350	0.4	10^6	61
CVD	N/A	N/A	450	14	10^2	62
CVD	N/A	N/A	550	29[b]	10^6	63
CVD	N/A	N/A	650	17[b]	10^6	64
CVD	N/A	Monolayer	700	45[c]	10^6	65
CVD	N/A	~0.7	750	1.8	10^4	66
CVD	N/A	~0.7	750	5	10^5	67
CVD	N/A	1.1	850	0.03	$<10^4$	68
CVD	N/A	~2.2	850	16	10^6	69
CVD	N/A	13–15 layers	900	67[c]	10^6	70
CVD	N/A	4 layers	900	1.3	10^6	71
CVD	N/A	~1.3	1000	0.01	10^2	72
CVD	N/A	~1.3	1000	0.1	10^2	73
CVD	N/A	2	1000	4.7	10^5	74

[a] N/A: not applicable; NMP: *N*-methyl-2-pyrrolidone; DMF: *N*,*N*-dimethylformamide. [b] High-*k*-dielectric. [c] Single crystal domain.

matches the interlayer distance of BP (0.53 nm); (2) the penetration and reduction of solvated protons ($HSO_4^- \leftrightarrow SO_4^{2-} + H^+$, $2H^+ + 2e^- \rightarrow H_2$) further increase the distance between two neighboring BP layers; and (3) the solvent propylene carbonate stabilizes the exfoliated flakes against reaggregation. Bottom-gate and bottom-contact field-effect transistors showed an excellent hole mobility of 252 ± 18 $cm^2 V^{-1} s^{-1}$ and a promising on/off ratio of $(1.2 \pm 0.15) \times 10^5$ at 143 K under vacuum. Our group reported an ultrafast (in minutes) cathodic expansion of bulk BP in the nonaqueous electrolyte of tetraalkylammonium salts.[85] A high-yield (>80%) production of nonoxidative few-layer phosphorene (FLBP) flakes with high crystallinity and thin thickness (average 5 layers) was achieved (Fig. 4a). The representative large-scale TEM image and the corresponding lattice further demonstrated the high-quality of FLBP (Fig. 4b and c). Besides, different alkyl-ammonium ions (TBA^+, tetramethylammonium, and tetraoctylammonium) and electrolyte solvents (polar protic, non-polar and polar aprotic) for intercalation were also investigated. The representative field-effect transistor (FET) devices as illustrated in Fig. 4d revealed a high hole mobility up to ~100 $cm^2 V^{-1} s^{-1}$ with a high on/off ratio (Fig. 4e and f). A comparison of the device characteristics of a thin layer BP FET with other reports is summarized in Table 2, which gives persuasive evidence of the superiority of electrochemical exfoliation. By taking advantage of this promising strategy, some unique artificial structures could be obtained. For example, Wang and co-workers reported an electrochemical molecular intercalation strategy to create a new class of artificial superlattices in which monolayer atomic phosphorene crystals alternate with molecular layers of cetyl-trimethylammonium bromide.[40] The interlayer distance of the obtained monolayer phosphorene molecular superlattices was more than double that in black phosphorus, and thus efficiently isolated the phosphorene monolayers. Importantly, a device made using this superlattice architecture achieved an on/off current ratio exceeding 10^7. Besides, quaternary ammonium molecules with different sizes and symmetries could also be intercalated into other 2D atomic crystals, such as MoS_2 and WSe_2, resulting in the generation of a broad class of superlattices with tailored molecular structures, interlayer distances, phase compositions, and electronic and optical properties.

Monolayer VSe_2 (1T and 2H phase), which has high Curie temperature (T_c) due to its strong electron coupling in the $3\ d^1$ odd-electronic configuration of V^{4+}, is another air-sensitive material. Motivated by the successful electrochemical exfoliation of 2D black phosphorus using organic ammonium cations as the intercalants, Yu *et al.* successfully performed tetrapropylammonium (TPA) chloride/propylene carbonate-based electrochemical exfoliation of 1T-VSe_2. AFM results indicated that more than 90% of the VSe_2 flakes had between one and five layers with an average lateral size of ≈40 μm (Fig. 4g and h). The atomic-resolution STEM image of a few-layer VSe_2 flake revealed the octahedral 1T phase (Fig. 4i). In the presence of an in-plane magnetic field, obvious magnetic hysteresis loops were observed at both 10 and 300 K, providing direct evidence for the ferromagnetism of the exfoliated VSe_2 sample (Fig. 4j).Though great achievement has been achieved, the exfoliated 2D VSe_2 is still extremely unstable in air and easily oxidized to form vanadium oxides (V_2O_5). XPS results of the exfoliated VSe_2 ultrathin nanosheets revealed that the Se/V stoichiometry ratio was around 1.84, suggesting the presence of Se vacancies, which may be the origin of the air instability as metallic atoms with unpaired electrons are prone to oxidation. Then, thiol molecules were further introduced onto the VSe_2 surface to passivate the exfoliated flakes, which improved the air stability of the flakes for subsequent characterization (Fig. 4k). A much-

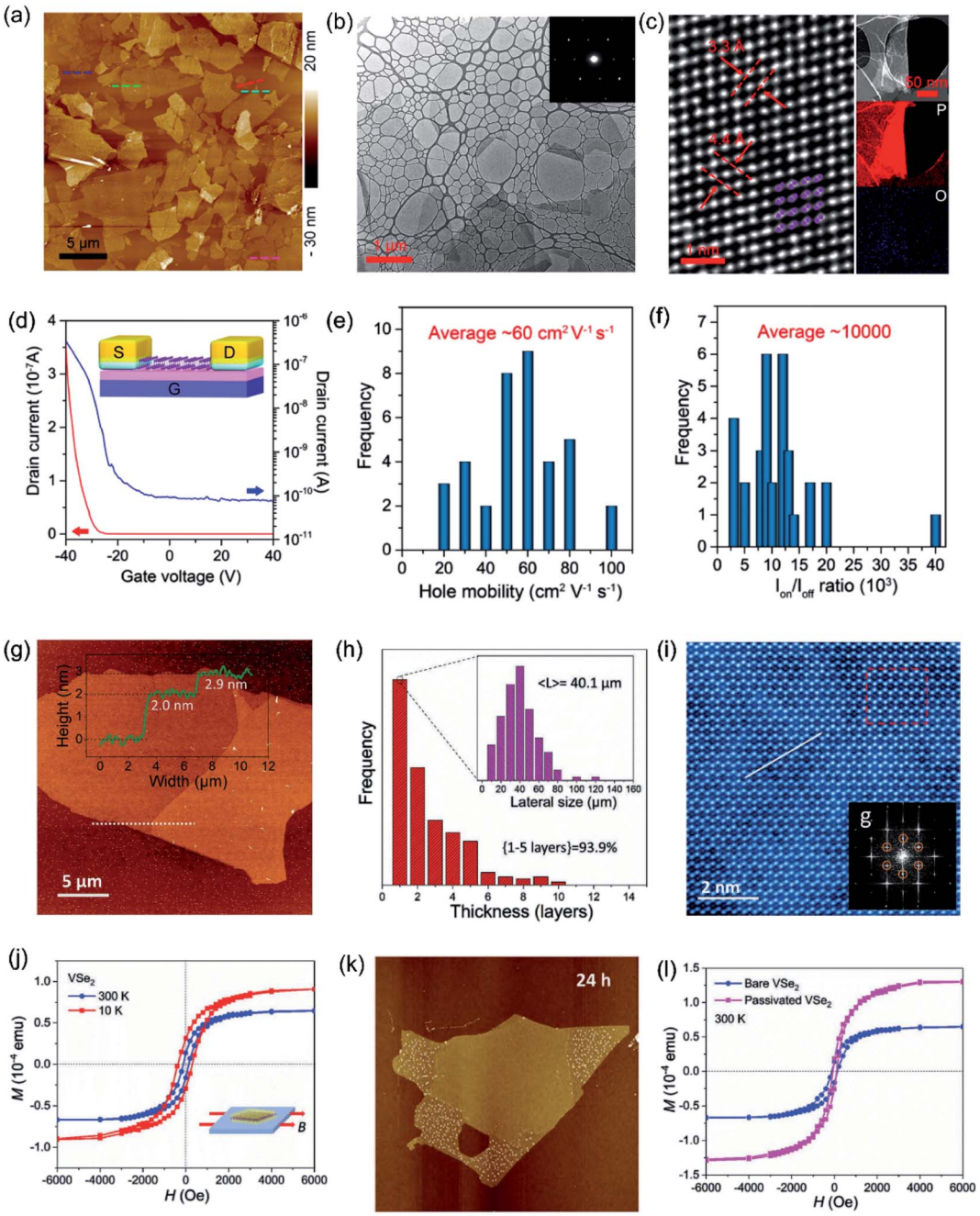

Fig. 4 Electrochemical cathodic exfoliation to prepare atomically thin air-sensitive materials such as 2D BP and VSe_2 nanosheets with high quality. (a) AFM image of FLBP flakes deposited onto a SiO_2/Si substrate. (b) TEM image of large-scale FLBP flakes with the corresponding selected area electron diffraction (SAED) pattern. (c) HRTEM and TEM-electron energy loss spectroscopy (TEM-EELS) images of the FLBP. (d) A representative charge transport curve for an FLBP FET device with the schematic illustration of an as-fabricated device. (e and f) Histograms of the hole-mobility and on/off ratio for the FLBP FET devices. Reproduced from ref. 85 with permission from Wiley-VCH, copyright 2018. (g) AFM topography images of stepped monolayer/bilayer VSe_2 flakes with the height profile. (h) Statistical histograms for the thickness distributions of exfoliated ultrathin VSe_2 flakes and (inset histogram) lateral size distributions of VSe_2 monolayers. (i) Atomic-resolution STEM image of an exfoliated VSe_2 flake. (j) M–H hysteresis loop of bare VSe_2 flakes on a SiO_2 substrate under an in-plane magnetic field at 300 and 10 K. (k) AFM topography images of passivated monolayer/bilayer VSe_2 flakes after exposure to the ambient environment for 14 h. (l) M–H hysteresis loops of bare and passivated VSe_2 flakes at 300 K. Reproduced from ref. 86 with permission from Wiley-VCH, copyright 2019.

enhanced M_s of 1.3×10^{-4} emu was obtained for the passivated samples compared to that of the bare sample (0.7×10^{-4} emu) at a similar coercive field (H_c) ($\approx$120 Oe) (Fig. 4l).

Some novel 2D materials can also be exfoliated. In 2017, Lu *et al.* reported the first electrochemical cathodic exfoliation of antimonene nanosheets.[93] The obtained few-layer antimonene nanosheets possessed an average thickness of 31.6 nm, a giant

Table 2 A summary of the device characteristics of thin layer BP FET devices

Exfoliation methods	BP thickness	Hole mobility	I_{on}/I_{off}	Temperature (K)	Channel length	Ref.
Electrochemical exfoliation	**4 ± 2.3 nm**	**60 ± 12**	**(1 ± 0.49) × 10^4**	**300**	**10–20**	85
Mechanical exfoliation	18.7 nm	170.5	300	300	3	87
Mechanical exfoliation	15 nm	600	10^5	300	1	12
Mechanical exfoliation	5 nm	205	10^5	120	1	12
Mechanical exfoliation	2 nm	50	5 × 10^5	120	1	12
Mechanical exfoliation	10 nm	300	10^3	300	1.5	88
Mechanical exfoliation	10 nm	N/A	10^5	<200	1.5	88
Mechanical exfoliation	8.9 nm	74	10^3	300	0.2	79
Mechanical exfoliation	5 nm	286	10^4	300	0.2	89
Mechanical exfoliation	5 nm	55	10^5	300	1.6	11
Exfoliation in NMP	Few layers	25.9	1.6 × 10^3	300	0.1–3	90
Exfoliation in DMF	7.4 nm	0.58	10^3	300	0.4	91
Exfoliation in water	10 nm	242	5 × 10^3	300	2.7	92

nonlinear refractive index of $\approx 10^{-5}$ cm^2 W^{-1}, and excellent stability under ambient conditions for months, much better than their unstable counterpart phosphorene. Recently, a family of metal thio(seleno)phosphates (MTPs), in which metal cations stabilize a $[P_2S(Se)_6]^{4-}$ framework forming layers that are weakly bonded together through van der Waals interactions, were widely explored due to their intermediate-range bandgaps, 1.3–3.5 eV, and incipient ionic conductivity. Some of these compounds exhibit ferroic correlations of atomic positions and the corresponding ferroic ground states and

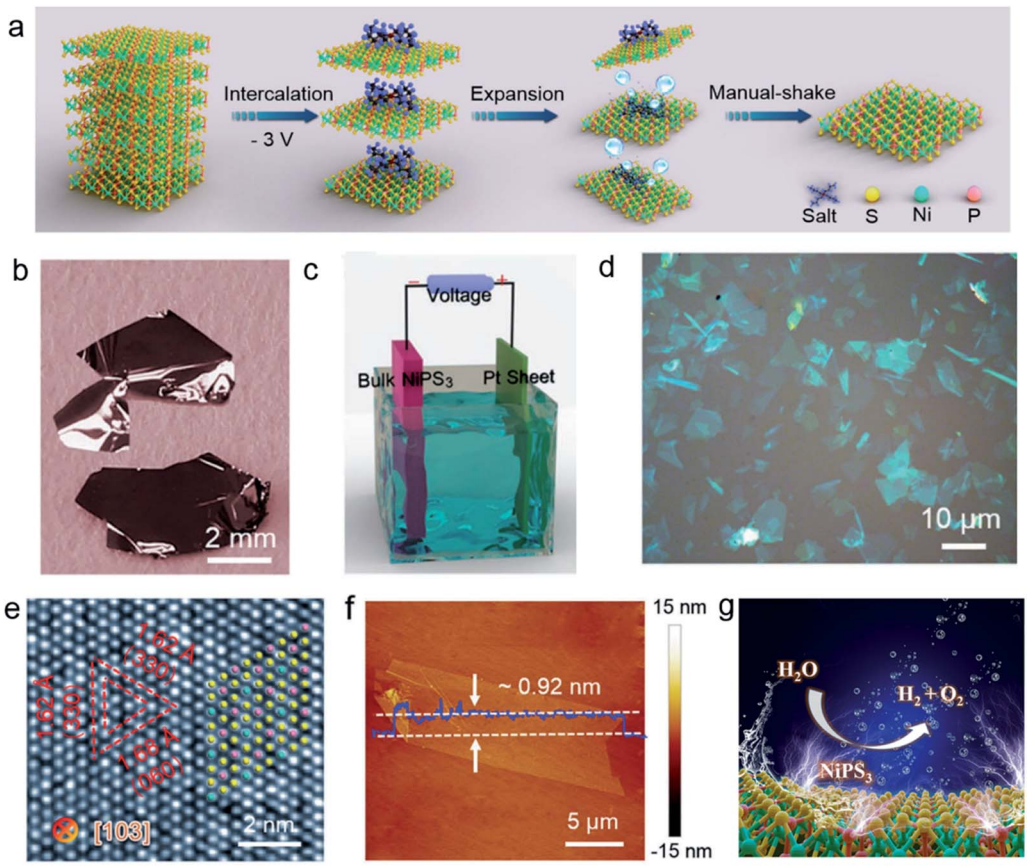

Fig. 5 Electrochemical cathodic exfoliation to prepare atomically thin 2D $NiPS_3$ flakes with high quality. (a) Illustration of the mechanism of electrochemically exfoliating bulk $NiPS_3$ crystals in TBA^+/DMSO electrolyte. (b) Photographs of the bulk $NiPS_3$ crystals synthesized by the CVT method. (c) Schematic illustration of the electrochemical exfoliation setup. (d) Optical microscopy image of high-coverage exfoliated $NiPS_3$. (e) HAADF-TEM image of exfoliated $NiPS_3$. (f) AFM image of exfoliated $NiPS_3$. (g) Schematic illustration of exfoliated $NiPS_3$ for water splitting. Reproduced from ref. 94 with permission from Wiley-VCH, copyright 2019.

associated phase transitions, yet others possess magnetic ordering. However, the production of monolayer and few-layer 2D MPT materials with high yield and quality is rarely reported. In 2019, large size and atomically thin $NiPS_3$ flakes with high crystallinity and a pure phase structure were prepared by electrochemical cathodic exfoliation in tetra-*n*-butylammonium salt/DMF electrolyte (Fig. 5).[94,95] The *in situ* video revealed that during the exfoliation process, the gaseous species generated from the decomposition of salts could efficiently expand the tightly stratified bulk $NiPS_3$ crystals. By slight manual shaking rather than sonication, atomically thin $NiPS_3$ flakes preserved the in-plane structural integrity with large size and minimum damage. As a result, large-sized ($\sim$150 μm^2) and thin layered ($\sim$70% monolayer) $NiPS_3$ flakes with high crystallinity and a pure phase structure with a yield approximately 80% were obtained. To the best of our knowledge, the electrochemical exfoliation reported here is the highest efficiency pathway for the preparation of large quantities of high-quality $NiPS_3$ with a large area and atomic thickness. More importantly, the exfoliated $NiPS_3$ sheets provided a brand-new and ideal model for overall water splitting because of their inherent fully exposed S and P atoms which are often the active sites for the HER and OER. Consequently, the bifunctional $NiPS_3$ sheets demonstrated promising performance for overall water splitting. Antimonene, a novel 2D group-VA material beyond phosphorene, has been theoretically predicted to possess promising electronics and optical properties with enhanced stability. Very recently, an ingenious electrochemical dual-electrode exfoliation strategy was precisely controlled by Zhang *et al.*,[96] and it can fabricate graphene with excellent yields (85% and 48% for the cathode and anode, respectively) comprising few-layer graphene (1–3 layers, >70%), ultralow defects (I_D/I_G < 0.08), and a high production rate (exceeding 25 g h^{-1}). When employed for inkjet printing, highly conductive (11 Ω sq^{-1}) and flexible graphene films can be obtained due to its excellent electrical conductivity (>3 $\times$ 10^4 S m^{-1}) and great solution dispersibility. Thus, this work will facilitate the development of large-scale production of high-quality graphene and holds great promise for its wide application.

In brief, cathodic exfoliation provides an advisable strategy to produce high-quality 2D materials with very large size, high crystallinity and a pure phase structure, comparable with those from the CVD method. Quaternary ammonium ions, a thionin acetate salt–NaCl couple,[97] ionic liquids,[98] aryl diazonium ions,[99] inorganic salts,[100] and inorganic acids,[101] are suitable intercalators for electrochemical cathodic exfoliation of bulk crystals, such as graphite,[97–99,102] MoS_2,[42] black phosphorus,[83,85,103] antimony,[100] and MXenes[104] (Table 3). However, it should be mentioned that catalytically active defects could also be introduced in some 2D materials *via* cathodic exfoliation. For example, abundant exposed basal planes and Mo vacancies could be formed in the outer layers of double transition metal MXene nanosheets ($Mo_2TiC_2T_x$) by cathodic electrochemical exfoliation, which could be employed to *in situ* immobilize single Pt atoms.[101] Besides, 2D few-layer Sb nanosheets with small size and a pure phase fabricated by cathodic exfoliation were excellent electrocatalysts for CO_2 reduction.[100] The extraordinary performance was ascribed to the high density of fully exposed edge defects.

3. Anodic exfoliation

Unlike cathodic intercalation, the anodic strategy allows *in situ* functionalization of exfoliated 2D sheets by positive potential-induced surface modification, oxidation, *etc.* During this process, the categories of intercalators selected have a decisive effect on the exfoliation and functionalization of targeted 2D sheets. For example, for the anodic exfoliation of graphite, organic salts, inorganic acids, bases, salts, and ionic liquids are commonly employed as intercalators and the choice of different intercalators will completely affect the type of functionalized graphene obtained. Wang *et al.* reported the electrochemical exfoliation of graphite to form graphene using poly(sodium-4-styrenesulfonate),[107] in which the edge-to-face interaction (π–π

Table 3 Reported intercalators for electrochemical cathodic exfoliation[a]

Intercalators	Solvent	Bulk crystals	Voltage	Thickness	Ref.
$LiClO_4$	PC	Graphite	-15 ± 5 V	1–5 layers	50
$LiPF_6$	EC/DMC	Graphite, MoS_2, WS_2, TiS_2, TaS_2, ZrS_2	0.05 mA	1 layer	51
$LiPF_6$	EC/DMC	BN, $NbSe_2$, WSe_2, Sb_2Se_3, Bi_2Te_3	0.025 mA	3–10 layers	52
TMA^+, TEA^+, TBA^+	NMP	HOPG	-5 V (*vs.* $Ag/AgClO_4$)	2–5 layers	54
$BMPTF_2N$	None	HOPG, graphite rods	15–30 V	2–5 layers	98
TBAP	DMF/MeCN	HOPG	-2.2 to -2.8 V (*vs.* Ag/Ag^+)	1–2 layers	99
$TBA{\cdot}PF_6$	DMF	BP crystals	-5 V	1–5 layers	83
$TBA{\cdot}BF_4$	DMSO	BP crystals	-5 V	5 layers	85
THAB	MeCN	MoS_2 crystals	-5 to -10 V	3.8 ± 0.9 nm	42
$TBA{\cdot}HSO_4$	PC	MoS_2 crystals	-5 V	6–10 layers	55
$TPA{\cdot}Cl$	PC	VSe_2 crystals	-4 V to -2 V	1–5 layers	105
Na_2SO_4	H_2O	Sb crystals	10 V	3.5 nm	100
Na_2SO_4	H_2O	Sb crystals	-6 V	31.6 nm	93
TBA^+	DMF	$NiPS_3$ crystals	-3 V	1–5 layers	106

[a] TMA^+: tetra-methyl-ammonium; TEA^+: tetra-ethyl-ammonium; TBA^+: tetra-*n*-butyl-ammonium; THAB: tetraheptylammonium bromide; TPA: tetrapropylammonium; $BMPTF_2N$: *N*-butyl, methylpyrrolidinium; bis(trifluoromethylsulfonyl)imide; NMP: 1-methyl-2-pyrrolidone; PC: propylene carbonate; EC: ethyl carbonate; DMC: dimethyl carbonate; MeCN: acetonitrile.

interaction) between the graphene surface and aromatic rings of poly(sodium-4-styrenesulfonate) was responsible for the successful exfoliation of a graphite electrode to graphene during the electrolysis. Afterward, sodium dodecyl benzene sulfonate (SDBS) revealed a similar capacity.[108,109] The presence of SO^{3-} was observed in the FTIR spectrum, pinpointing that the exfoliated graphene was functionalized with SDBS. Being an anionic surfactant, SDBS helped to achieve a uniform dispersion in water and prevented the π–π re-stacking. Later, single- and few-layer graphene, decorated with metal phthalocyanine molecules, were fabricated by electrolytic exfoliation of graphite in an electrolyte containing copper phthalocyanine-3,4′,4″,4‴-tetrasulfonic acid tetrasodium salt (TSCuPc).[110] Raman/FTIR/UV-Vis spectra and XRD revealed that the TSCuPc–graphene hybrid was formed by non-covalent π–π interactions between graphene sheets and metal phthalocyanine, and a high-quality graphene hybrid structure was achieved. Nitrogen-doped graphene quantum dots (N-GQDs) with oxygen-rich functional groups also can be prepared by the electrochemical method when employing TBA^+ as the intercalator.[111] When a positive potential was applied, the electrolyte was actuated into the graphene layers and the carbon–carbon double bonds of graphene were oxidized. The obtained physical and/or chemical defects along the graphene provided more active sites for preferential electrochemical oxidation, leading to the breakage of the graphene film into tiny graphene dots. Besides, N atoms could be *in situ* introduced into the resultant GQDs to form N-GQDs with oxygen-rich functionalities, as shown in Fig. 6. Completely different from their N-free counterparts, the exfoliated N-GQDs had a high N/C atomic ratio (*ca.* 4.3%) and could emit blue luminescence. Most importantly, they revealed an excellent performance in the oxygen reduction reaction (ORR) in an alkaline medium, even comparable to that of a commercial Pt/C catalyst. Electrochemically exfoliated graphene sheets can also be achieved by combining organic salts with inorganic salts, such as a 9-anthracene carboxylate ion–NaOH couple,[112] 6-amino-4-hydroxy-2-naphthalene–sulfonic acid–KOH couple,[113] and glycine–H_2SO_4 couple.[114]

When using inorganic acids as intercalators, anodic oxidation often occurred to produce exfoliated graphene materials with oxygen-functionalities. In 2011, Su *et al.* exfoliated graphite flakes or HOPG to mainly (60%) AB-stacked bi-layered graphene

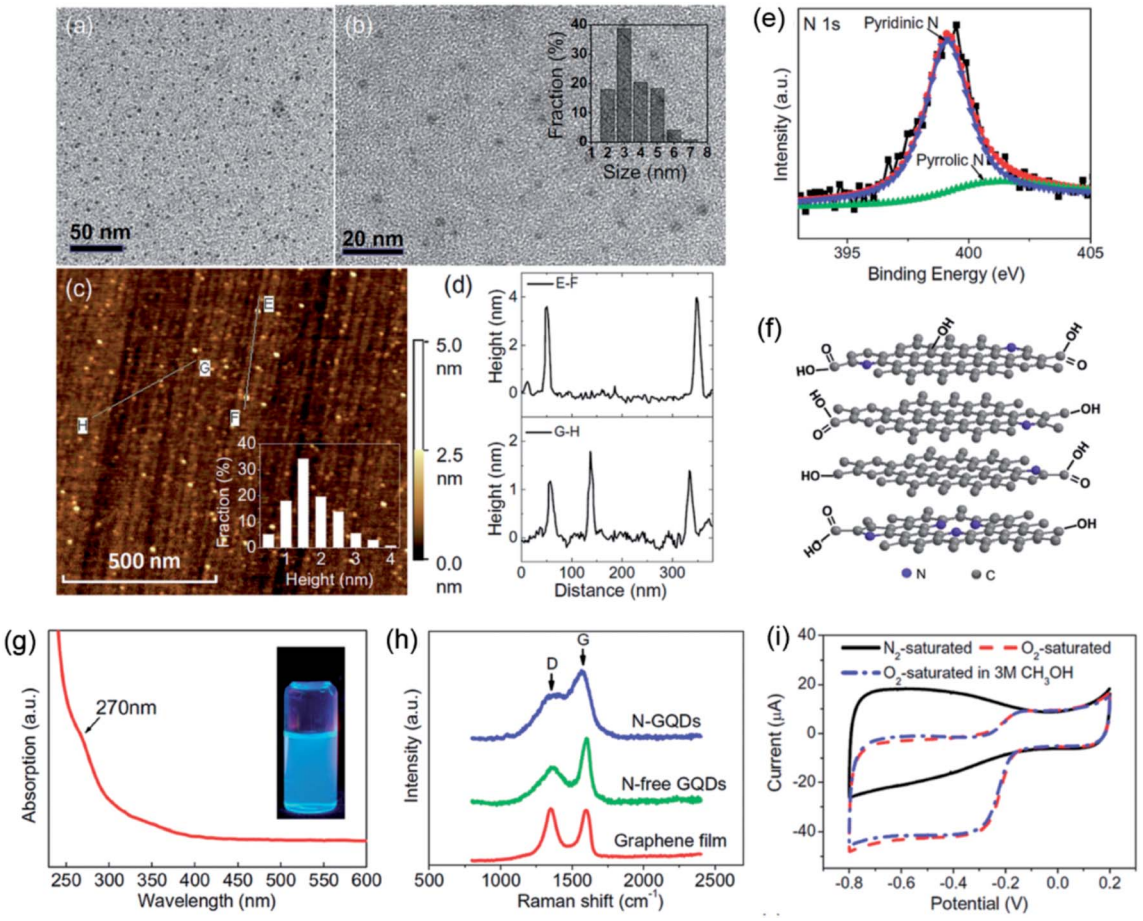

Fig. 6 Electrochemical exfoliation to prepare N-GQDs. (a and b) TEM images of the exfoliated N-GQDs under different magnifications. (c) AFM image of the N-GQDs on a Si substrate. (d) Height profile along the lines in (c). (e) High-resolution N 1s of N-GQDs. (f) The proposed structure of an O-rich N-GQD. (g) UV-vis absorption of N-GQDs in water. The inset is a photograph of the N-GQD solution in water under 365 nm UV irradiation. (h) Raman spectra of the original graphene film, N-free GQDs, and N-GQDs. (i) CV comparison of N-GQD/graphene and commercial Pt/C on a GC electrode. Reproduced from ref. 111 with permission from ACS Publications, copyright 2012.

in H_2SO_4 solution for the first time.[115] Later, Parvez *et al.* further demonstrated this strategy and proposed the exfoliation mechanism.[116] In their opinion, oxygen radicals ($O^{\bullet}$) and hydroxyl ($OH^{\bullet}$) generated from water oxidation ($H_2O \xrightarrow{e^-} H^+ + {}^{\bullet}OH \xrightarrow{e^-} H^+ + O$) led to the hydroxylation or oxidation of the graphite electrode at edge sites and grain boundaries. With the increase of time, anionic SO_4^{2-} intercalated into these defective sites, released gaseous SO_2 and/or led to anion depolarization, which caused the dramatic expansion of the interlayer distance of graphite. It is worth mentioning that the generation of oxygen or hydroxyl radicals during exfoliation can not only introduce oxygen-containing functional groups on the surface of exfoliated graphene but also provide an opportunity to fabricate graphene oxide (GO) if the oxidation degree of exfoliated graphene could be greatly improved. For anodic exfoliation, the anodic electrocatalytic oxygen evolution reaction of water occurs under an applied voltage, and it contains the following four elementary steps:

$$* + H_2O \xrightarrow{E} *OH + H^+ + e^- \quad (7)$$

$$*OH \xrightarrow{E} *O + H^+ + e^- \quad (8)$$

$$*OH + H_2O \xrightarrow{E} *OOH + H^+ + e^- \quad (9)$$

$$*OOH \xrightarrow{E} O_2 + H^+ + e^- \quad (10)$$

Here, * represents an active site on the electrode surface; *OH, *O, and *OOH refer to the radical intermediates adsorbed on the active site; and E stands for the applied voltage. For the electrochemical anodic exfoliation of graphite, the adsorbed reactive *OH, *O, and *OOH can react with the carbon lattice which is highly positively charged to form covalently bonded oxygen-containing functional groups. However, the rapid formation of a great amount of O_2 gas will exacerbate the exfoliation of the graphitic anode, leading to an ineffective current supply or a broken circuit and consequently stopping the electrochemical oxidation reaction.

Recently, Pei *et al.* demonstrated that the use of graphite intercalation compound paper (GICP) could efficiently inhibit the fast formation of O_2 at a high voltage.[41] As shown in Fig. 7, first, commercial flexible graphite paper (FGP) was electrochemically intercalated in concentrated H_2SO_4 to form stage-I GICP. Very surprisingly, the blue-colored GICP dipped in diluted 50 wt% H_2SO_4 could be quickly oxidized to yellow graphite oxide within a few seconds along with exfoliation. After vacuum filtration and rinsing with water, the filter cake was exfoliated in water by sonication to form a GO dispersion. The further analysis of gaseous products during the anodic exfoliation revealed that the mole ratio of O_2 to H_2 is only 1 : 8.36 for GICP as the anode, which is significantly smaller than that produced by water electrolysis with Pt (1 : 2.05) or FGP (1 : 3.4) as the anode. As a result, the exfoliation rate of GICP greatly increased and the graphite lattice could be fully oxidized within a few seconds to synthesize high-quality GO sheets by pre-intercalation of graphite in H_2SO_4 solution. This strategy is scalable, safe and green overcoming many disadvantages of the traditional chemical oxidation methods (Table 4), such as explosion hazard, environmental pollution, and long reaction times.

Inorganic bases are also applicable for the exfoliation and functionalization of graphene. In 2014, Rao *et al.* used NaOH/H_2O_2/H_2O incorporation to fabricate high-quality and few-layer graphene nanosheets with a high yield (95%).[124] They demonstrated that the presence of H_2O_2 significantly enhanced the exfoliation due to the formation of highly nucleophilic O_2^{2-}, produced for the intercalation and expansion process. In the absence of H_2O_2, the low-nucleophilic OH^- ions do not effectively intercalate and/or have poor interactions with graphite domains even under harsh conditions.

$$2OH^- + H_2O_2 \rightarrow O_2^{2-} + 2H_2O \quad (11)$$

Besides, different inorganic salts, such as phosphate buffer, $(NH_4)_2SO_4$, Na_2SO_4, K_2SO_4, and $LiClO_4$, have promptly exfoliated graphite into graphene with different features.[125–127] Parvez *et al.* proposed the corresponding mechanism:[126] first, the edge sites and grain boundaries of the graphite layers were attacked by the hydroxyl ions (OH^-), which were generated from water splitting after applying a potential to the electrode. Subsequently, two OH groups could interact with each other, forming epoxide rings. Alternatively, they could dissociate to form two carbonyl groups through additional oxidation (formula (12)–(14)). Second, the depolarization and expansion of the graphite layers occurred after the oxidation at the edge sites and grain boundaries, which lead to the intercalation of SO_4^{2-} and H_2O within the graphitic layers. Third, gaseous species, such as SO_2, O_2, and CO_2, were generated from the reduction of SO_4^{2-} anions and water oxidation, applying large forces on the graphite layers to peel off graphite layers from one another (formula (15) and (16)).

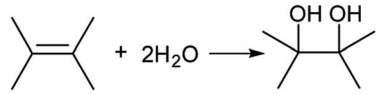

(12)

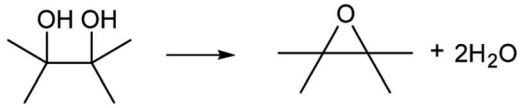

(13)

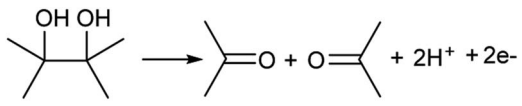

(14)

$$C + 2H_2O \rightarrow CO_2 + 4H^+ + 4e^- \quad (15)$$

$$2H_2O \rightarrow O_2 + 4H^+ + 4e^- \quad (16)$$

Heteroatoms (*e.g.*, O, N, B, S, and F) can also be incorporated into graphene lattices during the exfoliation process *via*

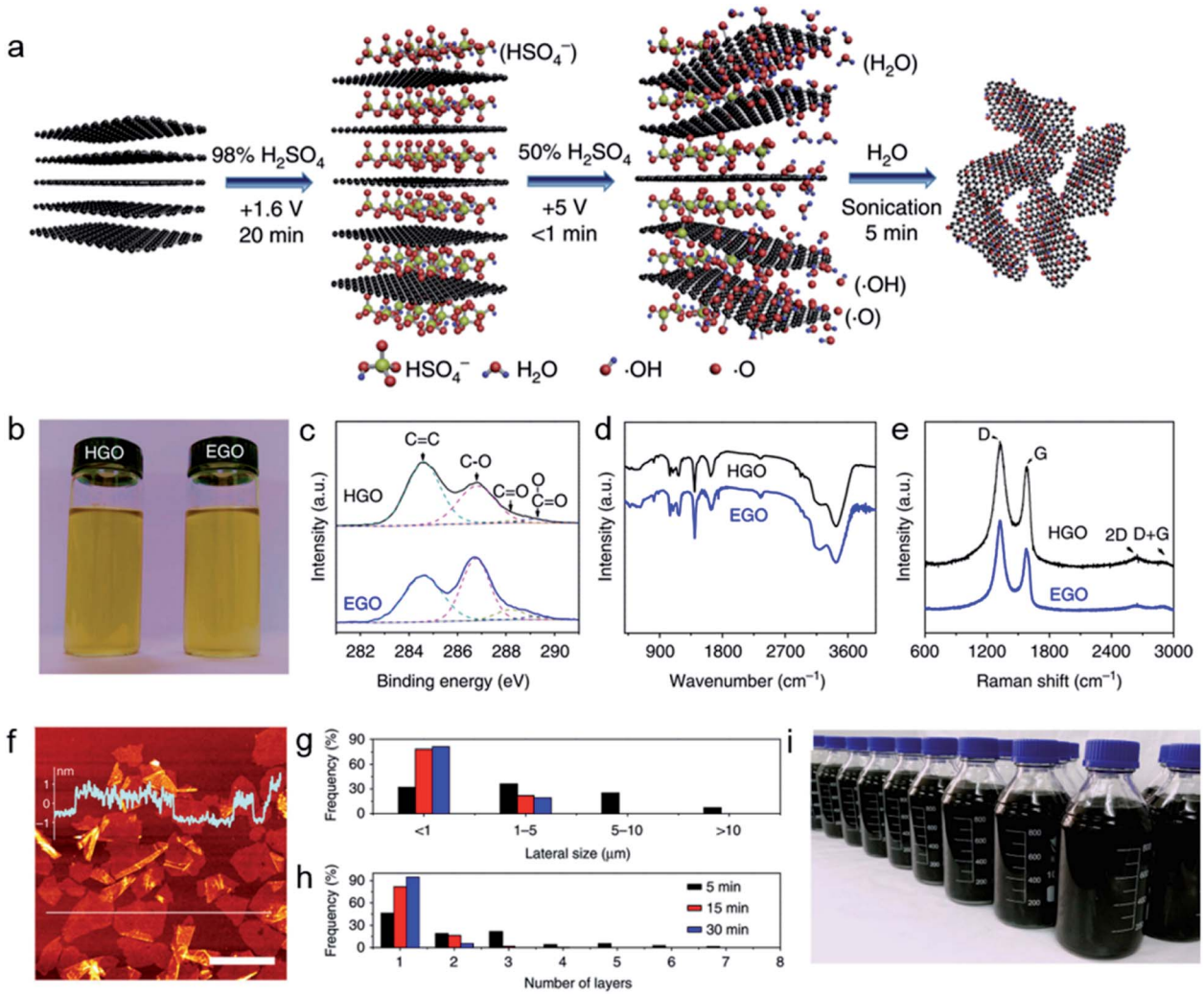

Fig. 7 Electrochemical anodic exfoliation to prepare functionalized graphene. (a) Schematic illustration of the preparation of electrochemically synthesized GO (EGO) by water electrolytic oxidation. (b) Comparison of EGO with GO synthesized by traditional Hummers' method (HGO) in aqueous solution (1 mg mL^{-1}). (c) XPS C 1s spectra of EGO and HGO. (d) FTIR spectra of EGO and HGO. (e) Raman spectra of EGO and HGO. (f) AFM image of EGO sheets. (g and h) Lateral size and the layer number distribution of EGO sheets obtained by sonication for 5 (black columns), 15 (red columns), and 30 min (blue columns). (i) Mass-produced EGO aqueous solution (5 mg mL^{-1}). Reproduced from ref. 41 with permission from Nature Publications, copyright 2018.

Table 4 Comparison of reaction parameters for GO synthesis by the electrochemical oxidation method and some typical traditional chemical oxidation methods[a]

Synthesis method	Reaction temperature	Reaction time to form graphite oxide	Ingredient consumption for 1 g graphite				
			H_2SO_4	Oxidant	Water	C/O	Ref.
Electrochemical exfoliation	**~20 °C**	**A few seconds**	**<0.43 mL**	**Radicals from water electrolysis**	**<150 g**	**1.5–1.8**	41
Modified Hummers' method	40 °C → 50 °C	>12 h	120 mL	H_3PO_4, $KMnO_4$	>267 g	N/A	117
Modified Hummers' method	<10 °C	>27 h	25 mL	$KMnO_4$, $NaNO_3$	>578 g	N/A	118
Modified Hummers' method	0 °C → 40 °C → 95 °C	>0.75 h	23 mL	$KMnO_4$	>292 g	2.36	119
Modified Hummers' method	80 °C → R.T. → 35 °C	>8.5 h	44 mL	$K_2S_2O_8$, P_2O_5, $KMnO_4$	>417 g	N/A	120
Strong oxidant method	R.T.	1 h	40 mL	K_2FeO_4	N/A	2.2	121
Modified Brodie method	0 °C → R.T.	96.5 h	17.5 mL	$KClO_3$, $fHNO_3$	>800 g	2.6	122
Modified Brodie method	R.T.	>24 h	N/A	$NaClO_3$, $fHNO_3$	N/A	2.8	123

[a] R.T.: room temperature; $fHNO_3$: fuming nitric acid.

inorganic salts, which further boost the electrochemical performance of the obtained graphene. Zhou *et al.* demonstrated that highly solution-processable and fluorine-modified graphene (FG) could be synthesized in a large scale by exfoliating graphite in a fluorine-containing neutral electrolyte (Fig. 8a).[128] The corresponding characterization revealed that the FG exhibited atomic thinness, a large lateral size (up to 12 μm), a high yield of >70% with ≤3 layers, and a fluorine doping of 3 at% (Fig. 8b). When assembled into flexible and high-energy-density ionogel-based micro-supercapacitors (FG-MSCs), it delivered a high energy density (56 mW h cm^{-3}), exceptional cyclability (~93% after 5000 cycles), and robust mechanical flexibility (100% capacitance retention when bent at 180°), surpassing most of the reported MSCs.

Ionic liquids have received dramatically increased interest in the past decade due to their negligible vapor pressure, low toxicity, high chemical and thermal stabilities, and diversity.[129,130] They also exhibit a relatively wide potential window and high conductivity,[131] and these properties are conducive to the electrochemical exfoliation of 2D materials. Liu *et al.* synthesized graphene nanosheets functionalized with an ionic liquid by exfoliating 1-octyl-3-methyl-imidazolium hexafluorophosphate ($[C_8mim]^+[PF_6]^-$)-treated graphite sheets.[132] Later, Lu *et al.* prepared fluorescent carbon nanoribbons, nanoparticles, and graphene sheets from the exfoliation of a graphite electrode in 1-butyl-3-methylimidazolium tetrafluoroborate ([BMIm][BF_4]).[133] The successful exfoliation was due to a complex interplay of anodic oxidation of water and anion intercalation from the ionic liquid. The proposed mechanism equations are represented as follows.

(1) The interaction between graphite (C_x) and water:

$$H_2O \rightarrow 2H^+ + 2e^- + 1/2O_2 \quad (17)$$

$$C_x + H_2O \rightarrow C_{1-x}OH + H^+ + e^- \quad (18)$$

$$C_x + 2H_2O \rightarrow C_{1-x} + CO_2 + 4H^+ + 4e^- \quad (19)$$

$$C_x + 2H_2O \rightarrow C_{1-x}COOH + CO_2 + 3H^+ + 3e^- \quad (20)$$

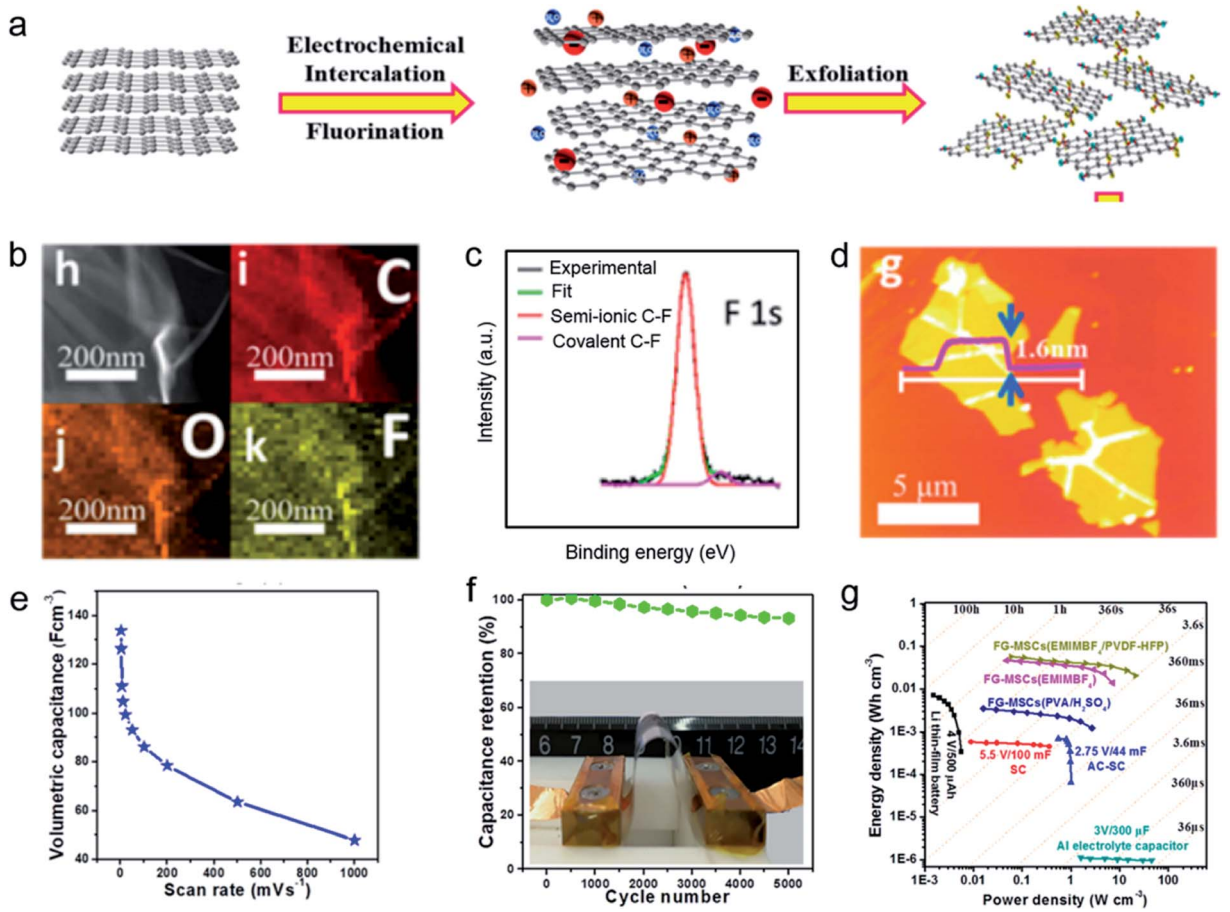

Fig. 8 Electrochemical anodic exfoliation to prepare fluorine-modified graphene (FG) nanosheets. (a) Illustration of electrochemical exfoliation of graphite to FG nanosheets in 0.1 M $NaBF_4$ aqueous electrolyte, *via* intercalation, fluorination, and exfoliation (red balls: BF^{4-} anions; blue balls: H_2O molecules). (b) Scanning transmission electron microscopy (STEM) image and carbon, oxygen, and fluorine elemental mapping images of exfoliated FG nanosheets. (c) F 1s XPS spectrum of FG nanosheets. (d) AFM image of FG nanosheets. (e) The volumetric capacitance of ionogel-based FG-MSCs. (f) Cycling stability of ionogel-based FG-MSCs under a constant bending state (inset: bent FG-MSCs). (g) Ragone plots of FG-MSCs in different electrolytes in comparison with those of a lithium thin-film battery (4 V/500 μA h), electrolytic capacitor (3 V/300 μF), and activated carbon supercapacitor (2.75 V/44 mF). Reproduced from ref. 128 with permission from ACS Publications, copyright 2018.

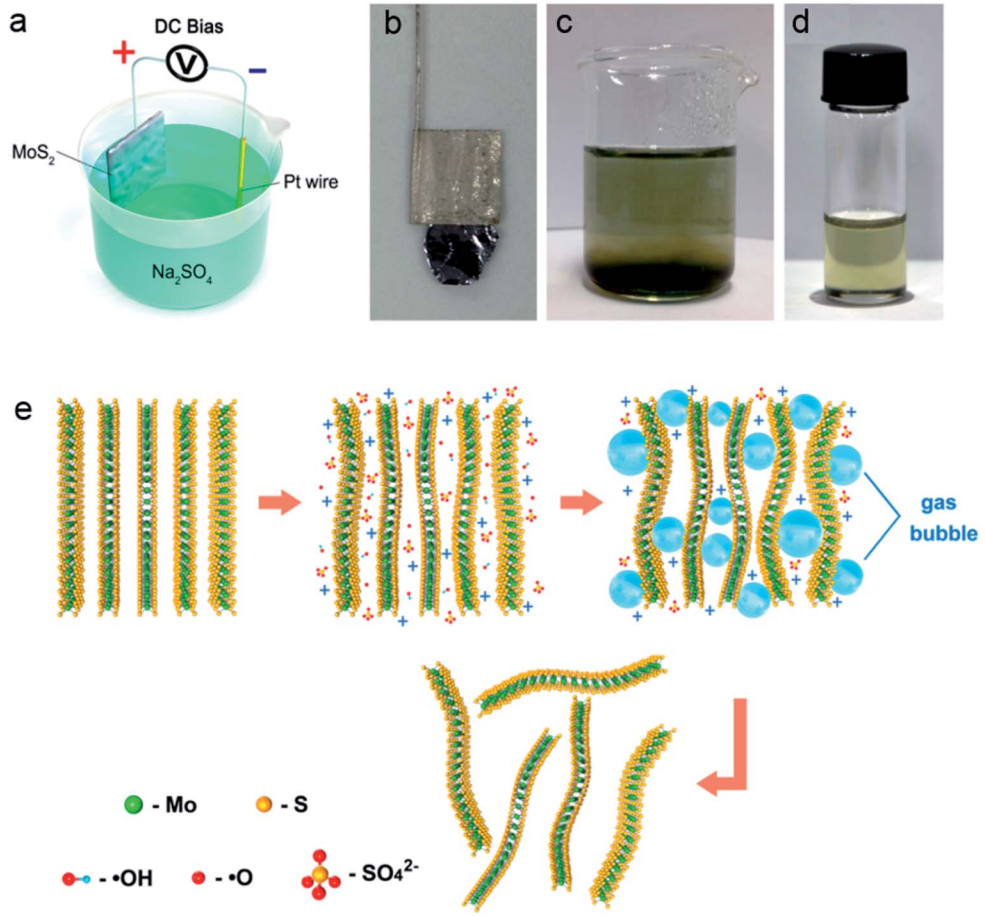

Fig. 9 Electrochemical anodic exfoliation to prepare MoS_2 nanosheets. (a) Illustration of electrochemical exfoliation of bulk MoS_2 crystals. (b) Photograph of a bulk MoS_2 crystal held by a Pt clamp before exfoliation. (c) Exfoliated MoS_2 nanosheets in Na_2SO_4 solution. (d) MoS_2 nanosheets in *N*-methyl-2-pyrrolidone solution. (e) Schematic illustration of the mechanism of electrochemical exfoliation of bulk MoS_2 crystals. Reproduced from ref. 135 with permission from ACS Publications, copyright 2014.

(2) The interaction between graphite and BF_4^-:

$$C_x + BF_4^- \rightarrow BF_4C_x + e^- \xrightarrow{H_2O} C_xOH + HBF_4 \quad (21)$$

First, anodic oxidation of water produces hydroxyl and oxygen radicals ($H_2O \xrightarrow{e^-} H^+ + \bullet OH \xrightarrow{e^-} H^+ + O\bullet$). Then, the oxidation of the edge planes opens up the edge sheets, facilitating intercalation of the anionic BF_4^-, which leads to the depolarization and expansion of the graphite anode. Furthermore, the BF_4 ion has a higher oxidation potential than water, and thus water will be sacrificially oxidized at the anode to generate hydroxyl and oxygen radicals. By increasing the ionic liquid/water ratio, the proportion of BF_4^- ions to water will be increased; this facilitates the intercalation process of BF_4^- and the expansion of the graphene anode. The heavily expanded graphite is more susceptible to oxidative cleavage to form nanoribbons. In contrast, increasing the water/ionic liquid content results in a larger concentration of OH and O radicals; these species oxidize the graphite anode which results in its dissolution as hydroxylated carbon particles. Recently, Wang *et al.* synthesized few-layer graphene flakes and isolated Fe atoms during the electrochemical exfoliation of graphite in the ionic liquid 1-butyl-3-methylimidazolium tetrachloro-ferrate.[134] The single Fe atoms were formed and anchored on exfoliated graphene after annealing $FeCl_4^-$-based intercalants in the presence of a nitrogen source.

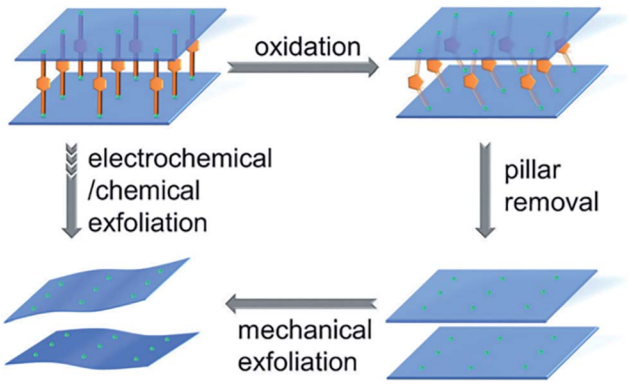

Fig. 10 Electrochemical anodic exfoliation of a pillared-layer MOF, copyright 2016. Reproduced from ref. 140 with permission from Wiley-VCH, copyright 2018.

Overall, organic salts, inorganic acids, bases, salts, and ionic liquids are extensively employed as intercalators in electrochemical anodic exfoliation of graphite. The choice of intercalators will determine the type of functionalized graphene obtained. When organic salts are employed as intercalators, the π–π interaction between the graphite and aromatic organic salts can contribute to the exfoliation process with the aid of electrochemical potential. Besides, the interaction between organic ions and inorganic ions can also promote the formation of ionic complexes and significantly enhance the intercalation process. Most importantly, due to the existing organic ions in the medium, the exfoliated graphene can be decorated by organic functional groups through noncovalent interaction, or heteroatoms *via* the doping effect. In addition, when inorganic acids, bases, and salts, and organic salts are used as intercalators, highly active oxygen radicals and OH˙ generated from water oxidation usually lead to the hydroxylation or oxidation of the graphite electrode at edge sites and grain boundaries, which provides the possibility of functionalizing the exfoliated graphene with oxygen groups. Such a situation can be further utilized to incorporate other heteroatoms (such as N, F, *etc.*) into the exfoliated graphene. Moreover, when ionic liquids are used as intercalators, there is a high possibility of producing single-atom anchored graphene.

Bulk MoS_2 crystals also can be electrochemically exfoliated through the anodic strategy. In 2014, You *et al.* employed electrochemical anodic exfoliation to prepare single or few-layer MoS_2 nanosheets in 0.5 M H_2SO_4 aqueous solution.[104] Soon afterward, Liu *et al.* chose neutral 0.5 M Na_2SO_4 aqueous solution as an electrolyte to exfoliate bulk MoS_2 crystals (Fig. 9).[135] Similar to the previously proposed mechanism for the exfoliation of graphite, once a positive potential is applied to the bulk MoS_2 specimen, oxidation of water around the bulk MoS_2 crystals will happen and generate abundant ˙OH and ˙O radicals. These radicals then insert into the MoS_2 layers along with SO_4^{2-} anions, and significantly weaken the van der Waals interactions. Afterward, gaseous species, such as O_2 and/or SO_2, will be generated after the oxidation of the radicals and/or

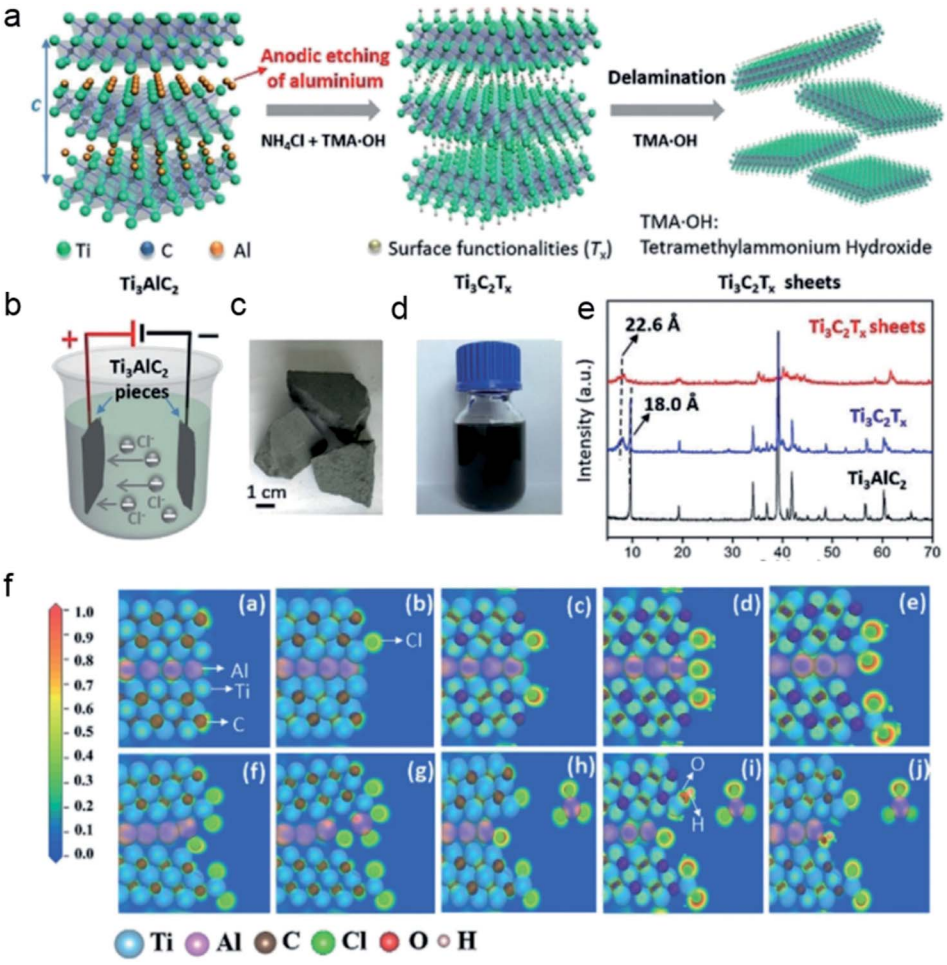

Fig. 11 Electrochemical anodic exfoliation to prepare $Ti_3C_2T_x$ nanosheets. (a) Schematic illustration of the etching and delamination process of bulk Ti_3AlC_2 in a binary aqueous electrolyte. (b) The configuration of the electrochemical cell. (c) Optical image of the original bulk Ti_3AlC_2 specimen. (d) The delaminated $Ti_3C_2T_x$ aqueous dispersion with a concentration of 0.15 mg mL^{-1}. (e) XRD patterns of Ti_3AlC_2, $Ti_3C_2T_x$, and $Ti_3C_2T_x$ films. (f) Electron localization function plots for pristine and etched Ti_3AlC_2 with the addition of 1–7 chloride anions, respectively. Reproduced from ref. 146 with permission from Wiley-VCH, copyright 2018.

anions, resulting in the great expansion of the MoS_2 interlayers. Finally, influenced by the driving force from the gaseous species, MoS_2 flakes are detached from the bulk MoS_2 crystals and suspended in the solution. Surprisingly, the lateral size of the MoS_2 nanosheets exfoliated electrochemically was up to 50 μm, much larger than that of MoS_2 nanosheets exfoliated *via* the liquid-phase. However, unlike the products from cathodic exfoliation of bulk MoS_2 crystals, the exfoliated MoS_2 nanosheets through the anodic strategy usually are partially oxidized.

Other 2D materials also can be obtained by electrochemical anodic exfoliation. Ambrosi proposed an anodic electrochemical exfoliation to exfoliate a BP crystal into nanosheets of reduced thickness.[136] The exfoliation efficiency and quality of the nanosheets in inorganic acidic aqueous solution were precisely controlled by adjusting the applied potential. However, the exfoliated BP presents a less intense P 2p signal. Besides, the signal centered at about 134 eV is more intense than that from the bulk BP crystal. These results revealed that the exfoliated nanosheets were easily oxidized *via* the anodic strategy. Appling the electrochemical anodic exfoliation strategy, single- and few-layer Bi_2Se_3 and Bi_2Te_3 sheets could also be prepared from natural Bi_2Se_3 and Bi_2Te_3 crystals in 0.5 M Na_2SO_4 aqueous solution.[137] These layered Bi_2Se_3 and Bi_2Te_3 materials are useful topological insulators due to their unique electronic and thermoelectric properties.[138,139] Very recently, Huang *et al.* have developed an electrochemical/chemical exfoliation strategy to synthesize 2D MOF materials based on coordination bonds (Fig. 10).[140] First, a novel 3D pillared-layer MOF ($(H_3O)_2[Co_6O(dhbdc)_2(H_2dhbdc)_2(EtOH)_4]_2\cdot EtOH$) was synthesized utilizing a catechol functionalized ligand as the redox active pillar. Then, the as-synthesized 3D pillared-layer MOF was used as an electrocatalyst for water oxidation. During the electrocatalysis process, the pillar ligands in MOFs can be *in situ* oxidized and removed, resulting in the formation of ultrathin (2 nm) 2D MOF layers. This *in situ* fabricated ultrathin 2D MOF shows exceptionally high OER activities, which are important for energy conversion.[141–144]

Using the electrochemical anodic exfoliation strategy, some elements in materials can be selectively etched during the exfoliation process. Zhao *et al.* employed the electrochemical anodic exfoliation strategy to selectively extract Ti from the MAX phase Ti_2SC to prepare multi-layers of C/S flakes with predominantly amorphous and some graphene-like structures.[145] Besides, covalent bonding between C and S was formed in the flakes, which revealed their promising potential as electrode materials for Li–S batteries. They also demonstrated that Ti could be extracted from other MAX phases, such as Ti_3AlC_2, Ti_3SnC_2, and Ti_2GeC. The results indicated that the electrochemical anodic exfoliation method could be an ingenious strategy to selectively etch the "M" elements from the MAX phases to fabricate an "AX" layered architecture, which shows promise for various applications, such as energy storage and catalysis. Yang *et al.* also synthesized $Ti_3C_2T_x$ (T = O, OH) (MXene) by employing the electrochemical anodic corrosion strategy (Fig. 11a–e).[146] By precisely controlling the corresponding electrolyte, the Al atoms could be selectively removed and substituted by hydroxide groups *in situ*, which leads to the generation of single or bilayer MXene sheets with a high yield (>90%) and large average dimensions. Density-functional theory (DFT) calculation revealed that the successful etching and *in situ* substitution were attributed to the positively charged anode, the interaction between Al atoms and Cl^-, the weak Ti–Al bonds, and the small ionic radius of OH^- (Fig. 11f).

$$Ti_3AlC_2 + 3Cl^- - 3e^- \rightarrow Ti_3C_2 + AlCl_3 \quad (22)$$

Table 5 Reported intercalators for electrochemical anodic exfoliation[a]

Intercalators	Solvent	Bulk crystals	Voltage	Thickness	Ref.
PSS	H_2O	Graphite rods	5 V	1–2 layers	107
SDBS	H_2O	Graphite rods	25 V	NA	109
TSCuPc	H_2O	Graphite rods	12 V	1–6 layers	110
ACA–NaOH	H_2O	Graphite rods	20 V	0.79 nm	112
$[C_8mim]^+Cl^-$	H_2O	Graphite rods	10–20 V	1.1 nm	132
$[BMIm][BF_4]$	H_2O	Graphite rods	1.515 V	NA	133
Glycine–H_2SO_4	H_2O	Graphite	NA	NA	114
H_2SO_4 or K_2SO_4	H_2O	HOPG or graphite	10 V	1–7 layers	115
H_2SO_4 (98 and 50 wt%)	H_2O	Flexible graphite paper	1.6 V to 5 V	<3 layers (86%)	41
$(NH_4)_2SO_4$ or Na_2SO_4 or K_2SO_4	H_2O	Graphite flakes	10 V	1–2 layers	126
$(NH_4)_2SO_4$ and TEMPO	H_2O	Graphite foil	10 V	1–3 layers	152
H_2SO_4 or Na_2SO_4 or $LiClO_4$	H_2O	Graphite foil	10 V	6–8 layer	127
$NaBF_4$	H_2O	Graphite foil	10 V	<3 layers (70%)	128
NaOH and H_2O_2	H_2O	Graphite rod	3V	3 layers	124
H_2SO_4	H_2O	MoS_2 crystals	10 V	1–3 layers	104
Na_2SO_4	H_2O	MoS_2 crystals	10 V	1–5 layers	135
H_2SO_4	H_2O	BP crystals	1 V to 3 V	NA	136
Na_2SO_4	H_2O	Sb crystals	10 V	3.5 nm	100

[a] PSS: poly(sodium-4-styrenesulfonate); SDBS: sodium dodecyl benzene sulfonate; TSCuPc: copper phthalocyanine-3,4′,4″,4‴-tetrasulfonic acid tetrasodium salt; $[C_8mim]^+Cl^-$: hydrophilic IL 1-octyl-3-methyl-imidazolium chlorine; $[BMIm][BF_4]$: 1-butyl-3-methylimidazolium tetrafluoroborate; ACA: 9-anthracene carboxylic acid; TEMPO: (2,2,6,6-tetramethylpiperidin-1-yl)oxyl; NA: not available.

The exfoliated $Ti_3C_2T_x$ sheets were utilized in an all-solid-state supercapacitor, which demonstrated outstanding areal and volumetric capacitances of 220 mF cm^{-2} and 439 F cm^{-3}, respectively, at a scan rate of 10 mV s^{-1}, superior to those of classic LiF/HCl-etched MXenes.[147–151]

In brief, electrochemical anodic exfoliation provides a new method to prepare functionalized 2D materials (Table 5). This strategy involves applying a positive bias to 2D crystals to induce the intercalation of negatively charged ions in the solution, along with any co-intercalating molecules, which can significantly increase the interlayer spacing between the individual sheets and lead to expansion and exfoliation. When the exfoliation process is carried out in aqueous solution, highly active radicals ($O^{\bullet}$ and $OH^{\bullet}$) from water electrolysis are usually generated due to the water oxidation reaction at the anode. These radicals can preferentially attack edge sites and grain boundaries, and functionalize the exfoliated 2D sheets with oxygen-containing groups. Besides, gaseous species (such as O_2), generated from the water oxidation, apply large forces on the crystals to increase the interlayer distance. Other non-metal heteroatoms, such as F, can also be doped into the exfoliated 2D materials when adding corresponding precursors to aqueous media, such as $NaBF_4$. By using the same strategy, such exfoliated 2D materials can be decorated with some organic molecules by incorporating organic salts into the electrolyte. When the process is carried out in organic solvents, the active radicals from water splitting can be avoided. In this kind of situation, organic salts, such as TBA^+, are usually used as intercalators, and the exfoliation mechanism is different from that in aqueous solution. In this case, organic cations with a smaller ionic diameter than the interlayer distance of the bulk crystals are directly inserted into the interlayers due to a positive electrochemical potential during the exfoliation process, causing a substantial augmentation in the interlayer spacing of the bulk crystals. The generated gases from the decomposition of organic cations can also significantly expand the tightly stratified bulk crystals. In this way, the exfoliated 2D materials can also be decorated by non-metal heteroatoms, such as N, when using N-containing intercalator precursors, such as TBA^+. Moreover, the anodically exfoliated 2D materials can be tailored to contain fluorescent and single-atom functionalities.

4. Conclusion and future perspectives

Electrochemical intercalation, which has been proven to be an effective strategy to fabricate ultrathin 2D materials from low-cost natural/synthetic bulk crystals, plays an important role in 2D science and practical applications. In this review, recent progress in the preparation of ultrathin 2D materials *via* electrochemical exfoliation has been classified and comprehensively examined. The general procedure is presented as follows: first, an applicable intercalator (*e.g.* organic salts, inorganic acids/bases/salts, ionic liquids, *etc.*) is chosen based on the desired structure of exfoliated 2D materials; second, actuating ionic species to intercalate into the interlamination of bulk 2D crystals by applying an electric potential, causing significant expansion of the tightly stratified bulk crystals and weakening the interlayer forces; third, a post-treatment process (*e.g.* transitory sonication, slight manual shaking, and centrifugation) to separate and release individual 2D sheets is used. Depending on the choice of intercalation or electric potential, the mechanism of exfoliation can be completely different. To sum up, for cathodic exfoliation, due to the possible phase transition caused by the Li-based cathodic intercalation, quaternary ammonium cations are the gentlest intercalators. During the exfoliation process, the electrons at the cathode have a reduction effect on the intercalated quaternary ammonium cations and provide a reductive environment for the exfoliated 2D materials. Thus, the obtained 2D materials usually possess high crystallinity, a pure phase structure, and negligible oxidation. In contrast, for anodic exfoliation, an aqueous solution system is usually employed. Thus, the oxygen radicals and hydroxyl generated from water oxidation provide a great possibility of functionalizing the exfoliated 2D materials with oxygen containing groups. Besides, the modification and element etching of the exfoliated materials also can be realized. In addition to these features, atomically thin 2D materials with large size and minimal damage can be obtained by a weak post-treatment method rather than sonication, which preserves the in-plane structural integrity.

Despite exciting achievements in the field of electrochemical exfoliation, some challenges remain. (1) Up to now, the electrochemical exfoliation method can only be applied to metallic or partially semiconducting 2D bulk crystals. Extending this approach to insulating or low-conducting layered materials remains a great challenge. (2) Regulating the characteristics of ultrathin 2D materials precisely (such as compositions, thicknesses, lateral sizes, crystal phases, doping, and surface features) during the exfoliation process is of paramount importance. Unfortunately, this is yet to be realized. (3) In most cases, ultrasonication is conducted in the post-treatment process after electrochemical exfoliation to improve the yield of monolayer and few-layer 2D materials. However, it may lower the quality of the final products for physical application. Thus, direct electrochemical exfoliation of bulk crystals into monolayer and few-layer 2D materials with high yield would be the best method and more work should be done. (4) Other 2D materials (such as perovskites, MPTs, MOFs, COFs, *etc.*) with fascinating properties (such as ferroelectricity, ferromagnetism, superconductivity, *etc.*) obtained through electrochemical exfoliation are underexploited and deserve more attention. (5) Though the electrochemical exfoliation method has been verified to work in a wide range of layered materials, most of the experiments are carried out on large-sized bulk single-crystals, which are expensive and impractical for industrial applications. As an alternative, small-sized powders or flakes, which are easily obtainable from natural mines or industrial synthesis, should be considered for effective and consecutive exfoliation. (6) Operando techniques to *in situ* monitor the process of electrochemical exfoliation are lacking, and a thorough investigation of the intercalation and exfoliation mechanism is urgently needed. If the above-mentioned challenges are solved,

it is expected that more electrochemically exfoliated 2D materials featuring special characteristics can be used for future applications.

Conflicts of interest

There are no conflicts to declare.

Acknowledgements

We acknowledge the support from the National Natural Science Foundation of China (No. 21972094, No. 21601193, No. 21703743), Research Foundation of China Postdoctoral Science (2018M630976), Guangdong Special Support Program, Pengcheng Scholar Program, Shenzhen Peacock Plan (Grant No. KQJSCX20170727100802505 and KQTD2016053112042971), and Educational Commission of Guangdong Province (2016KTSCX126).

References

1 K. S. Novoselov, A. K. Geim, S. V. Morozov, D. Jiang, Y. Zhang, S. V. Dubonos, *et al.*, *Science*, 2004, **306**, 666.
2 K. S. Novoselov, A. Mishchenko, A. Carvalho and A. H. Castro Neto, *Science*, 2016, **353**, aac9439.
3 J. R. Schaibley, H. Yu, G. Clark, P. Rivera, J. S. Ross, K. L. Seyler, *et al.*, *Nat. Rev. Mater.*, 2016, **1**, 16055.
4 A. J. Mannix, B. Kiraly, M. C. Hersam and N. P. Guisinger, *Nat. Rev. Chem.*, 2017, **1**, 0014.
5 H. Zhang, *Chem. Rev.*, 2018, **118**, 6089–6090.
6 C. Tan, X. Cao, X.-J. Wu, Q. He, J. Yang, X. Zhang, *et al.*, *Chem. Rev.*, 2017, **117**, 6225–6331.
7 Y. Chen, Z. Fan, Z. Zhang, W. Niu, C. Li, N. Yang, *et al.*, *Chem. Rev.*, 2018, **118**, 6409–6455.
8 D. Deng, K. S. Novoselov, Q. Fu, N. Zheng, Z. Tian and X. Bao, *Nat. Nanotechnol.*, 2016, **11**, 218.
9 C. Su and K. P. Loh, *Acc. Chem. Res.*, 2013, **46**, 2275–2285.
10 T. Sun, G. Zhang, D. Xu, X. Lian, H. Li, W. Chen, *et al.*, *Mater. Today Energy*, 2019, **12**, 215–238.
11 L. Li, Y. Yu, G. J. Ye, Q. Ge, X. Ou, H. Wu, *et al.*, *Nat. Nanotechnol.*, 2014, **9**, 372.
12 F. Xia, H. Wang and Y. Jia, *Nat. Commun.*, 2014, **5**, 4458.
13 Q. H. Wang, K. Kalantar-Zadeh, A. Kis, J. N. Coleman and M. S. Strano, *Nat. Nanotechnol.*, 2012, **7**, 699.
14 M. Chhowalla, H. S. Shin, G. Eda, L.-J. Li, K. P. Loh and H. Zhang, *Nat. Chem.*, 2013, **5**, 263.
15 X. Xu, W. Yao, D. Xiao and T. F. Heinz, *Nat. Phys.*, 2014, **10**, 343.
16 F. Song and X. Hu, *Nat. Commun.*, 2014, **5**, 4477.
17 G. Fan, F. Li, D. G. Evans and X. Duan, *Chem. Soc. Rev.*, 2014, **43**, 7040–7066.
18 M. A. Susner, M. Chyasnavichyus, M. A. McGuire, P. Ganesh and P. Maksymovych, *Adv. Mater.*, 2017, **29**, 1602852.
19 X. Li, X. Wu and J. Yang, *J. Am. Chem. Soc.*, 2014, **136**, 11065–11069.
20 J. Liu, X. Li, Y. Xu, Y. Ge, Y. Wang, F. Zhang, *et al.*, *Nanoscale*, 2019, **11**, 14383–14391.
21 T. Rodenas, I. Luz, G. Prieto, B. Seoane, H. Miro, A. Corma, *et al.*, *Nat. Mater.*, 2014, **14**, 48.
22 M. Zhao, Y. Wang, Q. Ma, Y. Huang, X. Zhang, J. Ping, *et al.*, *Adv. Mater.*, 2015, **27**, 7372–7378.
23 A. J. Clough, J. W. Yoo, M. H. Mecklenburg and S. C. Marinescu, *J. Am. Chem. Soc.*, 2015, **137**, 118–121.
24 J. W. Colson, A. R. Woll, A. Mukherjee, M. P. Levendorf, E. L. Spitler, V. B. Shields, *et al.*, *Science*, 2011, **332**, 228.
25 E. L. Spitler and W. R. Dichtel, *Nat. Chem.*, 2010, **2**, 672.
26 Y. Peng, Y. Huang, Y. Zhu, B. Chen, L. Wang, Z. Lai, *et al.*, *J. Am. Chem. Soc.*, 2017, **139**, 8698–8704.
27 K. Leng, I. Abdelwahab, I. Verzhbitskiy, M. Telychko, L. Chu, W. Fu, *et al.*, *Nat. Mater.*, 2018, **17**, 908–914.
28 J. C. Blancon, H. Tsai, W. Nie, C. C. Stoumpos, L. Pedesseau, C. Katan, *et al.*, *Science*, 2017, **355**, 1288.
29 M. Xu, T. Liang, M. Shi and H. Chen, *Chem. Rev.*, 2013, **113**, 3766–3798.
30 A.-Y. Lu, H. Zhu, J. Xiao, C.-P. Chuu, Y. Han, M.-H. Chiu, *et al.*, *Nat. Nanotechnol.*, 2017, **12**, 744.
31 J. Li, G. Zhan, Y. Yu and L. Zhang, *Nat. Commun.*, 2016, **7**, 11480.
32 J. Wu, H. Yuan, M. Meng, C. Chen, Y. Sun, Z. Chen, *et al.*, *Nat. Nanotechnol.*, 2017, **12**, 530.
33 K. Kim, S. Y. Lim, J.-U. Lee, S. Lee, T. Y. Kim, K. Park, *et al.*, *Nat. Commun.*, 2019, **10**, 345.
34 A. D. Oyedele, S. Yang, L. Liang, A. A. Puretzky, K. Wang, J. Zhang, *et al.*, *J. Am. Chem. Soc.*, 2017, **139**, 14090–14097.
35 W. L. Chow, P. Yu, F. Liu, J. Hong, X. Wang, Q. Zeng, *et al.*, *Adv. Mater.*, 2017, **29**, 1602969.
36 C. Tan, P. Yu, Y. Hu, J. Chen, Y. Huang, Y. Cai, *et al.*, *J. Am. Chem. Soc.*, 2015, **137**, 10430–10436.
37 J. Peng, J. Wu, X. Li, Y. Zhou, Z. Yu, Y. Guo, *et al.*, *J. Am. Chem. Soc.*, 2017, **139**, 9019–9025.
38 H. Song, T. Li, J. Zhang, Y. Zhou, J. Luo, C. Chen, *et al.*, *Adv. Mater.*, 2017, **29**, 1700441.
39 H. D. Yoo, Y. Liang, H. Dong, J. Lin, H. Wang, Y. Liu, *et al.*, *Nat. Commun.*, 2017, **8**, 339.
40 C. Wang, Q. He, U. Halim, Y. Liu, E. Zhu, Z. Lin, *et al.*, *Nature*, 2018, **555**, 231.
41 S. Pei, Q. Wei, K. Huang, H.-M. Cheng and W. Ren, *Nat. Commun.*, 2018, **9**, 145.
42 Z. Lin, Y. Liu, U. Halim, M. Ding, Y. Liu, Y. Wang, *et al.*, *Nature*, 2018, **562**, 254–258.
43 A. Ambrosi and M. Pumera, *Chem. Soc. Rev.*, 2018, **47**, 7213–7224.
44 C. Schafhaeutl, *J. Prakt. Chem.*, 1840, **21**, 129–157.
45 M. Inagaki, *J. Mater. Res.*, 2011, **4**, 1560–1568.
46 W. Rüdorff and U. Hofmann, *Z. Anorg. Allg. Chem.*, 1938, **238**, 1–50.
47 P. Yu, S. E. Lowe, G. P. Simon and Y. L. Zhong, *Curr. Opin. Colloid Interface Sci.*, 2015, **20**, 329–338.
48 M. S. Whittingham, *Science*, 1976, **192**, 1126.
49 B. K. Miremadi and S. R. Morrison, *J. Catal.*, 1991, **131**, 127–132.
50 J. Wang, K. K. Manga, Q. Bao and K. P. Loh, *J. Am. Chem. Soc.*, 2011, **133**, 8888–8891.

51 Z. Zeng, Z. Yin, X. Huang, H. Li, Q. He, G. Lu, *et al.*, *Angew. Chem., Int. Ed.*, 2011, **50**, 11093–11097.
52 Z. Zeng, T. Sun, J. Zhu, X. Huang, Z. Yin, G. Lu, *et al.*, *Angew. Chem., Int. Ed.*, 2012, **51**, 9052–9056.
53 W. Zhang, L. Sun, J. Marie, V. Nsanzimana and X. Wang, *Adv. Mater.*, 2018, **30**, 1705523.
54 A. J. Copper, N. R. Wilson, I. A. Kinloch and R. A. W. Dryfe, *Carbon*, 2014, **66**, 340–350.
55 P. Zhang, S. Yang, R. Pineda-Gómez, B. Ibarlucea, J. Ma, M. R. Lohe, *et al.*, *Small*, 2019, **15**, 1901265.
56 C. E. Dahm and D. G. Peters, *J. Electroanal. Chem.*, 1996, **402**, 91–96.
57 Q. He, Z. Zeng, Z. Yin, H. Li, S. Wu, X. Huang, *et al.*, *Small*, 2012, **8**, 2994–2999.
58 X. Yu, M. S. Prévot and K. Sivula, *Chem. Mater.*, 2014, **26**, 5892–5899.
59 A. G. Kelly, T. Hallam, C. Backes, A. Harvey, A. S. Esmaeily, I. Godwin, *et al.*, *Science*, 2017, **356**, 69.
60 J. Li, M. M. Naiini, S. Vaziri, M. C. Lemme and M. Östling, *Adv. Funct. Mater.*, 2014, **24**, 6524–6531.
61 Y. Xi, M. Isabel Serna, L. Cheng, Y. Gao, M. Baniasadi, R. Rodriguez-Davila, *et al.*, *J. Mater. Chem. C*, 2015, **3**, 3842–3847.
62 Y. R. Lim, W. Song, J. K. Han, Y. B. Lee, S. J. Kim, S. Myung, *et al.*, *Adv. Mater.*, 2016, **28**, 5025–5030.
63 K. Kang, S. Xie, L. Huang, Y. Han, P. Y. Huang, K. F. Mak, *et al.*, *Nature*, 2015, **520**, 656.
64 M. Zhao, Y. Ye, Y. Han, Y. Xia, H. Zhu, S. Wang, *et al.*, *Nat. Nanotechnol.*, 2016, **11**, 954.
65 H. Schmidt, S. Wang, L. Chu, M. Toh, R. Kumar, W. Zhao, *et al.*, *Nano Lett.*, 2014, **14**, 1909–1913.
66 T.-Y. Kim, M. Amani, G. H. Ahn, Y. Song, A. Javey, S. Chung, *et al.*, *ACS Nano*, 2016, **10**, 2819–2826.
67 L. Tao, K. Chen, Z. Chen, W. Chen, X. Gui, H. Chen, *et al.*, *ACS Appl. Mater. Interfaces*, 2017, **9**, 12073–12081.
68 A. Gurarslan, Y. Yu, L. Su, Y. Yu, F. Suarez, S. Yao, *et al.*, *ACS Nano*, 2014, **8**, 11522–11528.
69 J. Jeon, S. K. Jang, S. M. Jeon, G. Yoo, Y. H. Jang, J.-H. Park, *et al.*, *Nanoscale*, 2015, **7**, 1688–1695.
70 J. Zheng, X. Yan, Z. Lu, H. Qiu, G. Xu, X. Zhou, *et al.*, *Adv. Mater.*, 2017, **29**, 1604540.
71 X. Song, W. Zan, H. Xu, S. Ding, P. Zhou, W. Bao, *et al.*, *2D Materials*, 2017, **4**, 025051.
72 Y. Lee, J. Yang, D. Lee, Y.-H. Kim, J.-H. Park, H. Kim, *et al.*, *Nanoscale*, 2016, **8**, 9193–9200.
73 A. S. George, Z. Mutlu, R. Ionescu, R. J. Wu, J. S. Jeong, H. H. Bay, *et al.*, *Adv. Funct. Mater.*, 2014, **24**, 7461–7466.
74 K.-K. Liu, W. Zhang, Y.-H. Lee, Y.-C. Lin, M.-T. Chang, C.-Y. Su, *et al.*, *Nano Lett.*, 2012, **12**, 1538–1544.
75 D. Hanlon, C. Backes, E. Doherty, C. S. Cucinotta, N. C. Berner, C. Boland, *et al.*, *Nat. Commun.*, 2015, **6**, 8563.
76 A. K. Geim, *Science*, 2009, **324**, 1530.
77 A. Castellanos-Gomez, L. Vicarelli, E. Prada, J. O. Island, K. L. Narasimha-Acharya, S. I. Blanter, *et al.*, *2D Materials*, 2014, **1**, 025001.
78 S. Zhang, J. Yang, R. Xu, F. Wang, W. Li, M. Ghufran, *et al.*, *ACS Nano*, 2014, **8**, 9590–9596.
79 J. D. Wood, S. A. Wells, D. Jariwala, K.-S. Chen, E. K. Cho, V. K. Sangwan, *et al.*, *Nano Lett.*, 2014, **14**, 6964–6970.
80 M. Buscema, D. J. Groenendijk, S. I. Blanter, G. A. Steele, H. S. J. van der Zant and A. Castellanos-Gomez, *Nano Lett.*, 2014, **14**, 3347–3352.
81 T. Hong, B. Chamlagain, W. Lin, H.-J. Chuang, M. Pan, Z. Zhou, *et al.*, *Nanoscale*, 2014, **6**, 8978–8983.
82 R. Fei, A. Faghaninia, R. Soklaski, J.-A. Yan, C. Lo and L. Yang, *Nano Lett.*, 2014, **14**, 6393–6399.
83 Z. Huang, H. Hou, Y. Zhang, C. Wang, X. Qiu and X. Ji, *Adv. Mater.*, 2017, **29**, 1702372.
84 S. Yang, K. Zhang, A. G. Ricciardulli, P. Zhang, Z. Liao, M. R. Lohe, *et al.*, *Angew. Chem., Int. Ed.*, 2018, **57**, 4677–4681.
85 J. Li, C. Chen, S. Liu, J. Lu, W. P. Goh, H. Fang, *et al.*, *Chem. Mater.*, 2018, **30**, 2742–2749.
86 W. Yu, J. Li, T. S. Herng, Z. Wang, X. Zhao, X. Chi, *et al.*, *Adv. Mater.*, 2019, 1903779.
87 Y. Du, H. Liu, Y. Deng and P. D. Ye, *ACS Nano*, 2014, **8**, 10035–10042.
88 S. P. Koenig, R. A. Doganov, H. Schmidt, A. H. Castro Neto and B. Özyilmaz, *Appl. Phys. Lett.*, 2014, **104**, 103106.
89 L. Han, A. T. Neal, Z. Zhu, Z. Luo, X. Xu, D. Tománek, *et al.*, *ACS Nano*, 2014, **8**, 4033–4041.
90 J. Kang, J. D. Wood, S. A. Wells, J.-H. Lee, X. Liu, K.-S. Chen, *et al.*, *ACS Nano*, 2015, **9**, 3596–3604.
91 P. Yasaei, B. Kumar, T. Foroozan, C. Wang, M. Asadi, D. Tuschel, *et al.*, *Adv. Mater.*, 2015, **27**, 1887–1892.
92 L. Chen, G. Zhou, Z. Liu, X. Ma, J. Chen, Z. Zhang, *et al.*, *Adv. Mater.*, 2016, **28**, 510–517.
93 L. Lu, X. Tang, R. Cao, L. Wu, Z. Li, G. Jing, *et al.*, *Adv. Opt. Mater.*, 2017, **5**, 1700301.
94 X. Li, Y. Fang, J. Wang, B. Wei, K. Qi, H. Y. Hoh, *et al.*, *Small*, 2019, 1902427.
95 J. Liu, Y. Wang, Y. Fang, Y. Ge, X. Li, D. Fan, *et al.*, *Adv. Electron. Mater.*, 2019, 1900726.
96 Y. Zhang and Y. Xu, *Adv. Funct. Mater.*, 2019, **29**, 1902171.
97 M. Zhou, J. Tang, Q. Cheng, G. Xu, P. Cui and L.-C. Qin, *Chem. Phys. Lett.*, 2013, **572**, 61–65.
98 Y. Yang, F. Lu, Z. Zhou, W. Song, Q. Chen and X. Ji, *Electrochim. Acta*, 2013, **113**, 9–16.
99 I. Jeon, B. Yoon, M. He and T. M. Swager, *Adv. Mater.*, 2018, **30**, 1704538.
100 F. Li, M. Xue, J. Li, X. Ma, L. Chen, X. Zhang, *et al.*, *Angew. Chem., Int. Ed.*, 2017, **56**, 14718–14722.
101 J. Zhang, Y. Zhao, X. Guo, C. Chen, C.-L. Dong, R.-S. Liu, *et al.*, *Nat. Catal.*, 2018, **1**, 985–992.
102 Y. Zhang and Y. Xu, *Adv. Funct. Mater.*, 2019, 1902171.
103 S. Yang, K. Zhang, A. G. Ricciardulli, P. Zhang, Z. Liao, M. R. Lohe, *et al.*, *Angew. Chem., Int. Ed.*, 2018, **57**, 4677–4681.
104 X. You, N. Liu, C. J. Lee and J. J. Pak, *Mater. Lett.*, 2014, **121**, 31–35.
105 W. Yu, J. Li, T. S. Herng, Z. Wang, X. Zhao, X. Chi, *et al.*, *Adv. Mater.*, 2019, **31**, 1903779.
106 X. Li, Y. Fang, J. Wang, B. Wei, K. Qi, H. Y. Hoh, *et al.*, *Small*, 2019, **15**, 1902427.

107 G. Wang, B. Wang, J. Park, Y. Wang, B. Sun and C. Yao, *Carbon*, 2009, **47**, 3242–3246.
108 P. Li, S. H. Bae, Q. Y. Zan, N. H. Kim and J. H. Lee, *Adv. Mater. Res.*, 2010, **123–125**, 743–746.
109 E. H. Joo, T. Kuila, N. H. Kim, J. H. Lee, S. A. Kim, E. G. Park, *et al.*, *Adv. Mater. Res.*, 2013, **747**, 246–249.
110 J. P. Mensing, T. Kerdcharoen, C. Sriprachuabwong, A. Wisitsoraat, D. Phokharatkul, T. Lomas, *et al.*, *J. Mater. Chem.*, 2012, **22**, 17094–17099.
111 Y. Li, Y. Zhao, H. Cheng, Y. Hu, G. Shi, L. Dai, *et al.*, *J. Am. Chem. Soc.*, 2012, **134**, 15–18.
112 P. Khanra, T. Kuila, S. H. Bae, N. H. Kim and J. H. Lee, *J. Mater. Chem.*, 2012, **22**, 24403–24410.
113 T. Kuila, P. Khanra, N. H. Kim, S. K. Choi, H. J. Yun and J. H. Lee, *Nanotechnology*, 2013, **24**, 365706.
114 K. Sanjeeva Rao, J. Sentilnathan, H.-W. Cho, J.-J. Wu and M. Yoshimura, *Adv. Funct. Mater.*, 2015, **25**, 298–305.
115 C.-Y. Su, A.-Y. Lu, Y. Xu, F.-R. Chen, A. N. Khlobystov and L.-J. Li, *ACS Nano*, 2011, **5**, 2332–2339.
116 K. Parvez, R. Li, S. R. Puniredd, Y. Hernandez, F. Hinkel, S. Wang, *et al.*, *ACS Nano*, 2013, **7**, 3598–3606.
117 D. C. Marcano, D. V. Kosynkin, J. M. Berlin, A. Sinitskii, Z. Sun, A. Slesarev, *et al.*, *ACS Nano*, 2010, **4**, 4806–4814.
118 S. Eigler, M. Enzelberger-Heim, S. Grimm, P. Hofmann, W. Kroener, A. Geworski, *et al.*, *Adv. Mater.*, 2013, **25**, 3583–3587.
119 J. Chen, B. Yao, C. Li and G. Shi, *Carbon*, 2013, **64**, 225–229.
120 S.-T. Yang, Y. Chang, H. Wang, G. Liu, S. Chen, Y. Wang, *et al.*, *J. Colloid Interface Sci.*, 2010, **351**, 122–127.
121 L. Peng, Z. Xu, Z. Liu, Y. Wei, H. Sun, Z. Li, *et al.*, *Nat. Commun.*, 2015, **6**, 5716.
122 H. C. Schniepp, J.-L. Li, M. J. McAllister, H. Sai, M. Herrera-Alonso, D. H. Adamson, *et al.*, *J. Phys. Chem. B*, 2006, **110**, 8535–8539.
123 H.-J. Shin, K. K. Kim, A. Benayad, S.-M. Yoon, H. K. Park, I.-S. Jung, *et al.*, *Adv. Funct. Mater.*, 2009, **19**, 1987–1992.
124 K. S. Rao, J. Senthilnathan, Y.-F. Liu and M. Yoshimura, *Sci. Rep.*, 2014, **4**, 4237.
125 F. Zeng, Z. Sun, X. Sang, D. Diamond, K. T. Lau, X. Liu, *et al.*, *ChemSusChem*, 2011, **4**, 1587–1591.
126 K. Parvez, Z.-S. Wu, R. Li, X. Liu, R. Graf, X. Feng, *et al.*, *J. Am. Chem. Soc.*, 2014, **136**, 6083–6091.
127 A. Ambrosi and M. Pumera, *Chem.–Eur. J.*, 2016, **22**, 153–159.
128 F. Zhou, H. Huang, C. Xiao, S. Zheng, X. Shi, J. Qin, *et al.*, *J. Am. Chem. Soc.*, 2018, **140**, 8198–8205.
129 C. Hardacre, J. D. Holbrey, M. Nieuwenhuyzen and T. G. A. Youngs, *Acc. Chem. Res.*, 2007, **40**, 1146–1155.
130 T. Welton, *Chem. Rev.*, 1999, **99**, 2071–2084.
131 P. Hapiot and C. Lagrost, *Chem. Rev.*, 2008, **108**, 2238–2264.
132 N. Liu, F. Luo, H. Wu, Y. Liu, C. Zhang and J. Chen, *Adv. Funct. Mater.*, 2008, **18**, 1518–1525.
133 J. Lu, J.-X. Yang, J. Wang, A. Lim, S. Wang and K. P. Loh, *ACS Nano*, 2009, **3**, 2367–2375.
134 J. Wang, H. Zhang, C. Wang, Y. Zhang, J. Wang, H. Zhao, *et al.*, *Energy Storage Materials*, 2018, **12**, 1–7.
135 N. Liu, P. Kim, Ji H. Kim, J. H. Ye, S. Kim and C. J. Lee, *ACS Nano*, 2014, **8**, 6902–6910.
136 A. Ambrosi, Z. Sofer and M. Pumera, *Angew. Chem., Int. Ed.*, 2017, **56**, 10443–10445.
137 A. Ambrosi, Z. Sofer, J. Luxa and M. Pumera, *ACS Nano*, 2016, **10**, 11442–11448.
138 G. Zhou and D. Wang, *Sci. Rep.*, 2015, **5**, 8099.
139 J. N. Coleman, M. Lotya, A. O'Neill, S. D. Bergin, P. J. King, U. Khan, *et al.*, *Science*, 2011, **331**, 568.
140 J. Huang, Y. Li, R.-K. Huang, C.-T. He, L. Gong, Q. Hu, *et al.*, *Angew. Chem.*, 2018, **130**, 4722–4726.
141 X. Li, Y. Fang, X. Lin, M. Tian, X. An, Y. Fu, *et al.*, *J. Mater. Chem. A*, 2015, **3**, 17392–17402.
142 X. Li, Y. Fang, S. Zhao, J. Wu, F. Li, M. Tian, *et al.*, *J. Mater. Chem. A*, 2016, **4**, 13133–13141.
143 X. Li, Y. Fang, F. Li, M. Tian, X. Long, J. Jin, *et al.*, *J. Mater. Chem. A*, 2016, **4**, 15501–15510.
144 X. Li, Y. Fang, L. Wen, F. Li, G. Yin, W. Chen, *et al.*, *Dalton Trans.*, 2016, **45**, 5575–5582.
145 M.-Q. Zhao, M. Sedran, Z. Ling, M. R. Lukatskaya, O. Mashtalir, M. Ghidiu, *et al.*, *Angew. Chem., Int. Ed.*, 2015, **54**, 4810–4814.
146 S. Yang, P. Zhang, F. Wang, A. G. Ricciardulli, M. R. Lohe, P. W. M. Blom, *et al.*, *Angew. Chem.*, 2018, **130**, 15717–15721.
147 H. Hu, Z. Bai, B. Niu, M. Wu and T. Hua, *J. Mater. Chem. A*, 2018, **6**, 14876–14884.
148 H. Hu and T. Hua, *J. Mater. Chem. A*, 2017, **5**, 19639–19648.
149 S. Jiao, A. Zhou, M. Wu and H. Hu, *Adv. Sci.*, 2019, **6**, 1900529.
150 N. Kurra, B. Ahmed, Y. Gogotsi and H. N. Alshareef, *Adv. Energy Mater.*, 2016, **6**, 1601372.
151 Y.-Y. Peng, B. Akuzum, N. Kurra, M.-Q. Zhao, M. Alhabeb, B. Anasori, *et al.*, *Energy Environ. Sci.*, 2016, **9**, 2847–2854.
152 S. Yang, S. Brüller, Z.-S. Wu, Z. Liu, K. Parvez, R. Dong, *et al.*, *J. Am. Chem. Soc.*, 2015, **137**, 13927–13932.